JOURNAL PRE-PROOF

ofioliti
An International Journal
on Ophiolites and Modern Oceanic Lithosphere

LATE CRETACEOUS ARC MAGMATISM IN THE SOUTHERN CENTRAL PONTIDES: CONSTRAINTS FOR THE CLOSURE OF THE NORTHERN NEOTETHYAN BRANCHES

Kaan Sayit, M. Cemal Göncüoğlu, Alessandro Ellero, Giuseppe Ottria,
Chiara Frassi, Michele Marroni and Luca Pandolfi

To appear in OFIOLITI
DOI: https://doi.org/10.4454/ofioliti.v47i1.549

Received date: 25 March 2021
Accepted date: 18 October 2021
First published online 10 November 2021

LATE CRETACEOUS ARC MAGMATISM IN THE SOUTHERN CENTRAL PONTIDES: CONSTRAINTS FOR THE CLOSURE OF THE NORTHERN NEOTETHYAN BRANCHES

Kaan Sayit*,✉, M. Cemal Göncüoğlu*, Alessandro Ellero, Giuseppe Ottria**, Chiara Frassi***, Michele Marroni***, ** and Luca Pandolfi***, ****

* *Department of Geological Engineering, Middle East Technical University, 06800 Ankara, Turkey.*
** *Istituto di Geoscienze e Georisorse - CNR, Via G. Moruzzi 1, 56124, Pisa, Italy.*
*** *Dipartimento di Scienze della Terra, Università di Pisa, via S. Maria 53, 56126, Pisa, Italy.*
✉ *Corresponding author, e-mail: michele.marroni@unipi.it*

Keywords: *andesites; volcanic arc; geodynamics; Neotethys Ocean; Central Pontides; Northern Turkey.*

ABSTRACT

In the southern Central Pontides in northern Turkey the remnants of two Neotethyan oceanic basins, currently represented by the Intra-Pontide and the Izmir-Ankara-Erzincan sutures, and the interposing continental microplate (i.e., the Sakarya Composite Terrane) are completely dissected by the North Anatolian Shear Zone (NASZ). Within the resulting kilometre-scale, strike-slip fault-bounded blocks, several Late Cretaceous arc-type magmatic units have been detected. In this paper, we present new geochemical data from one of these magmatic units, the Yerkuyu Unit, that forms an ENE-WSW trending 30-km long and 10-km wide lens-shaped body surrounded by the splays of the NASZ.

The studied igneous lithologies have a subduction-related magmatic geochemical signature matching with another lozenge-shaped magmatic block: Tafano Unit. However, the tectono-magmatic characterization indicates that the Tafano Unit magmatism developed within a continental arc tectonic setting, while the volcanic rocks of the Yerkuyu Unit derived from oceanic arc magmatism. This finding indicates that the subducted oceanic lithosphere of the İzmir-Ankara-Erzincan branch of the Neotethys Ocean produced oceanic volcanic arcs close to the subduction zone (i.e., the Yerkuyu Unit) and beneath the Sakarya continental microplate (i.e., the Tafano Unit).

INTRODUCTION

The present-day tectonic setting of Turkey is an assemblage of several continental microplates separated by ophiolite-bearing suture zones (Sengör and Yılmaz, 1981; Göncüoğlu et al., 1997; Okay and Tüysüz, 1999). This setting is the result of a long-lived geodynamic history started in the Triassic and characterized by the closure of several oceanic basins and the consequent collision and amalgamation of several Gondwana-derived microplates.

The southern Central Pontide region (central-northern Turkey) is an intricated area where the imbricated remnants of two Neotethyan oceanic basins and an intervening continental microplate crop out along a N-S geotraverse of about 100 km. This structural setting is additionally strongly

dismembered by the presence of the North Anatolian Shear Zone (NASZ, Şengör et al., 2005; Ellero et al., 2015a), a complex Cenozoic kilometre-wide crustal-scale deformation zone.

The northernmost of these suture zones (i.e., the Intra-Pontide Suture, IPS, zone) derives from the closure of the Intra-Pontide Ocean (IPO), a wide oceanic area located between the Sakarya Microcontinent or Sakarya Composite Terrane (SKT), at the south, and the Eurasia continental margin, today represented by the Istanbul-Zonguldak terrane (IZT), at the north. This closure was probably generated in the Late Triassic to Early Cretaceous time span by multiple events of subduction and obduction each of which produced accretionary wedge and several volcanic arcs all along the subduction zones (Şengör and Yılmaz, 1981; Göncüoğlu et al., 1987; Yılmaz, 1990; Göncüoğlu and Erendil, 1990; Yılmaz et al., 1997; Ustaömer and Robertson, 1999; Okay and Tüysüz, 1999; Elmas and Yiğitbaş, 2001; Robertson and Ustaömer, 2004; Göncüoğlu et al., 2008; Robertson et al., 2013; Marroni et al., 2014; 2020; Aygül et al., 2015; 2016; Sayit et al., 2016; Frassi et al., 2016; 2018). The southernmost suture zone represents the remnant of the Izmir-Ankara-Erzincan Ocean (IAEO, Şengör and Yılmaz, 1981; Göncüoğlu et al., 2000; Okay and Tüysüz, 1999) located between the SKT and the Tauride-Anatolide Continental Microplate (or terrane) of Gondwanan affinity. Disregarding its debated pre-Mesozoic history (see Göncüoglu, 2019 and Okay et al., 2020), it is commonly accepted that the IAEO basin opened in the Triassic or even Permian (e.g., Göncüoğlu et al., 2010; Sayit et al., 2017; Tekin et al., 2019) and closed in the Paleocene. Its closure occurred by multiple north-dipping subductions that produced several continental and oceanic volcanic arcs (Tüysüz et al., 1995; Yalınız et al., 1996; Speciale et al., 2012; Aygül et al., 2015; Okay et al., 2020).

To unravel the geodynamic history of the Southern Central Pontides, it is fundamental to study the volcanic rocks exposed at present-day as lozenge-shaped blocks bounded by the NASZ faults. These rocks, formed during the numerous events of subductions, are conventionally interpreted as derivative of melts formed by partial melting of the mantle wedge metasomatized via subduction (e.g., Ringwood, 1974; Gill, 1981; Plank and Langmuir, 1988; Stern, 1991; Davidson and Tepley, 1997; Annen et al., 2006; Streck et al., 2007; Reubi and Blundy, 2009; Kent et al., 2010; Stern, 2011; Lee and Bachmann, 2014; Hacker et al., 2015; Stern et al., 2019; Straub et al., 2020). Hence, detailed structural and stratigraphic studies, age correlation and geochemical features of each volcanic body exposed in the Central Pontide area may help to decipher the nature, the pristine position, and orientation of the subduction zones and the IPO and/or IAEO before their closure.

In this paper, we present a new data set about Late Cretaceous volcanic arc rocks (i.e., the Yerkuyu Unit) preserved in a lozenge-shaped block within the NASZ, located between Ilgaz and Tosya (Figs. 1 and 2) and their comparison with those available in the literature for the closest non-metamorphic volcanic arc block exposed 25-30 km to the southwest (i.e., the Tafano Unit: Ellero et al., 2015b). We also suggest a geodynamic scenario for the lower Late Cretaceous magmatic arc volcanism along the southern margin of Eurasia plate.

GEODYNAMIC FRAMEWORK OF THE CENTRAL PONTIDES

The Central Pontides is an imbricate stack of oceanic and continental tectonic units including metamorphic, sedimentary, and igneous rocks ranging in age from Neo-Proterozoic to Cenozoic, that have experienced Cadomian, Variscan, Cimmeride, and Alpine orogenic events (Şengör and Yılmaz, 1981; Göncüoğlu et al., 1997; 2000; Okay and Tüysüz, 1999; Akbayram et al., 2013). Along a traverse from the Black Sea to Ankara and from the top to the bottom of the nappe pile are exposed the following units/structural complexes (Fig. 1): (1) the IZT, representing the southern margin of Eurasia, (2) the IPS zone whose final architecture was mainly resulted from the collision between the IZT and the SKT, (3) the SKT, of Gondwana affinity and, (4) the Izmir-

Ankara-Erzincan Suture (IAES) belt separating the SKT from the Gondwana-derived Tauride Anatolide Microplate.

The IZT consists of a Neoproterozoic and Variscan crystalline basement (Görür et al., 1997; Okay and Topüz, 2017; Göncüoğlu, 2019) covered by Permian to Late Triassic continental deposits, Late Jurassic-Early Cretaceous limestones (Aydın et al., 1995; Derman and Sayılı, 1995; Tüysüz, 1999; Okay et al., 2017) and Barremian-Aptian (Hippolyte et al., 2010) turbidite sequence (i.e., Çağlayan formation).

The IPS zone is an imbricated stack of variably metamorphic oceanic assemblages, known as the Central Pontides Structural Complex (CPSC) (Tekin et al., 2012) mainly consisting of 6 tectonic units: the Domuz Dağ Unit (DZU) (Tüysüz and Yiğitbaş, 1994; Ustaömer and Robertson, 1999; Okay et al., 2006; Frassi et al., 2016; Sayit et al., 2016; Aygül and Oberhänsli, 2017; Marroni et al., 2020), the Saka Unit (SKU) (Okay et al., 2013; Marroni et al., 2014; 2020; Sayit et al., 2016; Frassi et al., 2020), the Daday Unit (DDU) (Okay et al., 2013; Frassi et al., 2016; 2018; Sayit et al., 2016; Marroni et al., 2020), the Emirköy turbidite Unit (EMU) (Frassi et al., 2016), the Ayli Dağ ophiolite Unit (ADU) (Göncüoğlu et al., 2012) and the Arkot Dağ Mélange (AKM) (Tüysüz, 1990; Özcan et al., 2007 Göncüoğlu et al., 2014, Frassi et al., 2016; 2018; Okuyucu et al., 2017). DZU, SKU and DDU are affected by pervasive deformations and metamorphism acquired in a subduction setting under eclogite, high-pressure amphibolite and blueschists facies metamorphic conditions, respectively (Okay et al., 2006; 2013; Frassi et al., 2016; 2020; Aygül and Oberhänsli, 2017; Marroni et al., 2020). EMU, ADU and AKM are instead poorly deformed and affected by low- to very low-grade metamorphism. For a complete description and review of these units see Marroni et al. (2020).

The SKT has a Variscan and Cimmerian metamorphic basements unconformably covered by a non-metamorphic continental- to shallow-marine Early Jurassic clastic rocks, Middle Jurassic to Early Cretaceous neritic and pelagic limestones (Altıner et al., 1991) and Late Cretaceous to Middle Paleocene (Catanzariti et al., 2013) turbidite deposits of the Taraklı Flysch.

The IAES zone comprises variably deformed and metamorphosed Triassic-Late Cretaceous ophiolites, ophiolitic mélange complexes, bodies of volcanic arcs and continental margin sequences. The relationships between the IZT, IPS, SKT, and IAES units are unconformably sealed by the post-collisional sedimentary deposits whose inception is Late Paleocene in age (Özcan et al., 2007).

The NASZ, operating in the Central Pontides since the Early Eocene (e.g., Ottria et al., 2017), has deeply changed the geometry of the original nappe stacking through the development of strike-slip faults, folds, thrusts and pull-apart basins (Fig. 2). In this area, it roughly coincides with the IPS zone but also preserves fault-bounded blocks of the IAES zone, implying original proximity of the two oceanic sutures. The result of the NASZ activity is a randomly mix of ESE-WSW elongated fault-bounded blocks derived by the two Neotethys basins (IPO and IAEO) and the related continental margins (IZT and SKT).

Products of Late Cretaceous magmatism are widely exposed in the Central Pontides. The northernmost Late Cretaceous basaltic-andesitic volcanic belt is formed along the southern Black Sea coast. In the commonly accepted interpretation, it represents the remnants of a volcanic arc within the IZT, formed by the northward subduction of the IPO lithosphere beneath the Eurasian margin (e.g., Rice et al., 2006; Okay et al., 2013). On the contrary, there are arguments (e.g., Eyüboglu et al., 2013) ascribing the formation of this arc to the southward subduction of a Tethyan branch beneath an IZT-type Variscan continental crust.

Several Late Cretaceous arc-type magmatic fault-bounded blocks are recently differentiated as kilometre-scale fault-bounded blocks within the NASZ (Fig. 2) (Marroni et al., 2020). Only two of these arc-type magmatic blocks were studied in detail (the third, the Yerkuyu Unit, is the object of this study). The easternmost of them is the Kösdağ Unit (cfr. Kösdağ Metavolcanics in Tüysüz, 1990; Berber et al., 2014; 2021; Aygül et al., 2015) (Fig. 2), an approximately 40 km long and 10 km wide block bounded by the splays of the NASZ and sandwiched between CPSC

units in the north and the Ophiolitic Mélange of the IAES in the south. The unit consists of metabasalts, meta-andesites, and meta-rhyolites with well-developed blastomylonitic textures, covered by recrystallized Late Cretaceous pelagic limestones and metacherts. Geochemically, the metavolcanics of the Kösdağ Unit are represented by two distinct groups with subalkaline nature and subduction-related magmatic signatures. The trace element ratios indicate that they have derived from a depleted source modified by subduction component. Zircons from metarhyolites yielded LA-ICP-MS U-Pb ages between 94.64±0.77 Ma and 113.2±2.3 Ma (Berber et al., 2021). Berber et al. (2021) suggested that the Kösdağ Unit, together with structurally disrupted, but coeval island-arc type volcanic rocks in northern Central Anatolia, may testify the presence of an intra-oceanic subduction zone during the lower Late Cretaceous within the IAEO branch of the Neotethys Ocean.

The second studied arc-type magmatic body is represented by the Tafano Unit (Ellero et al., 2015b), located to the SW of the Kösdağ Metavolcanics and south of Tosya (Fig. 2). This unit consists of non-metamorphic basalts and basaltic andesites covered by volcaniclastic and sedimentary deposits. Preliminary geochemical data suggest that they belong to a magmatic arc developed on a thinned continental margin (Ellero et al., 2015b).

GEOLOGICAL FEATURES OF THE TAFANO AND YERKUYU UNITS

Stratigraphy

The Tafano and Yerkuyu units are exposed as lozenge-shaped blocks delimited by an anastomosed network of high-angle faults within the southern portion of the NASZ (Ellero et al., 2015a) (Fig. 2). Based on the lithological assemblages and mesostructural features, these two fault-bounded blocks were initially (erroneously) interpreted as fragments of a single arc-type magmatic tectonic unit, only differentiated by the volcanoclastic and sedimentary successions.

The Tafano Unit is characterized by volcanic complexes covered by well-developed volcaniclastic and sedimentary deposits. Three formations have been distinguished: i) the Basal Volcanic Complex, ii) the Volcaniclastic Sandstone Formation, and iii) the Marly-calcareous Turbidite Formation. The volcanic rocks consist of basalt, basaltic andesite, and andesite lava flows (Fig. 3a), associated with their pyroclastic equivalents, and cut by basaltic dikes and sills. Calcarenites and calcirudites are intercalated with the basalt, basaltic andesite, and dacite lava flows, and are interpreted as the products of the erosion of a carbonatic platform developed onto the volcanic arc during a volcanic inactivity period (Ellero et al., 2015b). These sediment layers prelude to the Volcaniclastic Sandstone Formation deposition, which starts with breccias characterized by volcanic and limestone clasts embedded in a silty matrix. The sedimentary succession continues upward with a turbidite sequence, consisting of alternations of arenites, siltites, grey marls and marly-siltitic shales. The turbidite sequence is also characterized by intercalated pebbly mudstones deposits, with quartz and carbonate clasts. The stratigraphic succession of Tafano Unit ends with the Marly-calcareous Turbidite Formation, consisting of calcareous turbidites and megaturbidites. The age of the Tafano Unit was obtained by calcareous nannofossil biostratigraphy, which suggests a late Santonian to middle Campanian age (Ellero et al., 2015b).

Differently from the Tafano Unit, the Yerkuyu Unit is mainly represented by a Volcanic Complex, consisting of an assemblage of basalt, basaltic andesite, and dacite flows (Fig. 3c) cut by subordinate basaltic dikes and sills whereas the sedimentary cover is represented by sporadic thin calcarenite layers (Fig. 3d) intercalated with lava flows in the upper part of Volcanic Complex.

Petrography

Basalts, basaltic andesites, and andesites were sampled from both the Tafano and Yerkuyu units, whereas dacites were only collected from the Yerkuyu Unit (Fig. 2, Table 1). Lithologies from both units are largely porphyritic with phenocrysts (up to 7 mm in length) embedded in a fine-grained pylotaxitic, trachytic, or intersertal groundmass. Aphyric texture is observed in both lavas and dykes. Low-grade hydrothermal alteration, which appear to have taken place under zeolite facies conditions, is present but varies within the units. Basaltic and andesitic varieties are characterized by a magmatic assemblage of plagioclase and clinopyroxene, while dacites include quartz and plagioclase.

Plagioclase occurs as a common phenocryst phase in all lithotypes, though it is more abundant in andesites and dacites than in basalts. Plagioclase is typically twinned in a polysynthetic fashion (Fig. 3e,f). Combined twins also occur and zoning is common. Plagioclase locally forms glomeroporphyritic clusters in andesites. Some plagioclase grains display resorption. Plagioclase is variably replaced by several secondary mineral phases, including epidote, prehnite, chlorite, sericite, zeolite, and calcite. Olivine is present as a phenocryst phase, but it is now totally replaced and occurs as pseudomorphs of chlorite and calcite. Clinopyroxene commonly displays subhedral outlines, and it is present mostly as a phenocryst phase. Twinning can be observed. Clinopyroxene is altered to a secondary assemblage of chlorite, epidote, and calcite. Quartz is the typical phenocryst phase of the Yerkuyu Unit dacites. It is commonly embayed and rounded, implying resorption by the melt. Opaque phases (Fe-Ti oxides) are also present. The groundmass appears to contain glass initially, but it is altered to chlorite, calcite, and zeolites. In some cases, the groundmass is oxidized. Vesicles occur, though not common, and they are filled chiefly by chlorite and zeolite.

Geochemistry and petrogenesis

Analytical method

Sample collection for geochemistry was performed simultaneously to detailed examination of the lithologies and deformation features during the fieldwork. We present here new whole-rock geochemical data from the igneous lithologies of the Yerkuyu Unit (Fig. 2). The new data include six samples analyzed at the ACME Laboratories (Canada) (http://acmelab.com/). Major oxides in addition to Ni and Sc were measured by lithium borate fusion ICP-ES, whereas remaining trace elements (including rare earth elements - REE) were measured by lithium borate fusion ICP-MS (except Pb, for which Aqua Regia digestion was used). Analyses of in-house standards and replicates revealed that accuracy was better than 6%, while precision was better than 3% for most major and trace elements. Loss on ignition (LOI) was determined by weight difference ignition at 1000°C. The Tafano Unit data are from Ellero et al. (2015b) and were also analyzed at the ACME Labs, following the same analytical procedure. This, therefore, allows a good comparison between the two data sets.

Assessment of alteration

The effect of low-grade hydrothermal alteration is reflected by the LOI values that vary within a large spectrum. Under such conditions, elements of low ionic potential such as Ba, Rb, K and Sr are generally known to be mobile, whereas elements of relatively high ionic potential (e.g., high field strength elements - HFSE and REE) are considered as immobile (e.g., Humphris and Thompson, 1978; Staudigel et al., 1996). In the multi-element plots (Fig. 5), the so called mobile LILE appear to be somewhat consistent, in general, which may suggest that they remained stable

to some extent. However, anomalous behaviour of these elements can also be found in some samples, attesting therefore their mobile nature in such cases. On the other hand, HFSE and REE display coherent patterns, indicating their relative immobility during post-magmatic processes. Therefore, our petrogenetic interpretations will be based mainly on the elements HFSE and REE, while mobile elements will be used with caution.

Results

Since the studied samples display evidence of low-degree hydrothermal alteration (which will be further evaluated in the discussion section), we prefer to use the classification diagram of Winchester and Floyd (1977) for a first-order classification. In this plot (Fig. 4), all the samples display sub-alkaline affinity, with a Nb/Y range between 0.05-0.57. However, a distinct separation between the two analyzed groups is notable; the Tafano Unit is completely isolated from the Yerkuyu Unit for its markedly higher Nb/Y ratios (0.37-0.57 and 0.05-0.14, respectively). In both groups, basaltic members are more dominant, with more evolved members being andesite/basaltic-andesite with higher Zr/TiO_2 ratios. While the compositional spectrum appears to be continuous in the Tafano Unit, the Yerkuyu Unit displays a gap, which can be an artifact of a lesser number of samples.

In the N-MORB-normalized multi-element plots (Sun and McDonough 1989) (Fig. 5), all studied samples display negative Nb anomalies, with high Th/Nb (Yerkuyu Unit: 0.25-0.80; Tafano Unit: 1.18-1.69) and La/Nb ratios (Yerkuyu Unit: 1.7-4.0; Tafano Unit: 1.9-3.7) (For N-MORB, Th/Nb = 0.05, La/Nb = 1.07). Apart from their redistribution (due to alteration) in some samples, the large ion lithophile elements (LILE) Sr, K, Ba and Rb are also enriched compared to HFSE and HREE. The Yerkuyu Unit samples appear to be more depleted than the Tafano Unit ones. This difference becomes even more drastic when the two evolved samples (15-TF-8 and 15-TF-11) from the Yerkuyu Unit are excluded. The Nb and Zr concentrations in the relatively primitive members of the Yerkuyu Unit are distinctly lower than that of average N-MORB (Nb_{MORB} = 0.26-0.43; Zr_{MORB} = 0.19-0.30; subscript "MORB" denotes N-MORB-normalized). The Tafano Unit samples, on the other hand, are variably enriched in terms of these elements relative to N-MORB (Nb_{MORB} = 2.1-6.1; Zr_{MORB} = 1.0-2.5). This difference observed in the enrichment levels between the samples of the two units also persists for Th and LREE. In the chondrite-normalized REE plots (Sun and McDonough 1989) (Fig. 5), all samples exhibit relatively flat HREE profiles ($[Dy/Yb]_N$ = 1.0-1.4). The LREE systematics, however, change between the groups. The Yerkuyu Unit displays somewhat flat REE patterns for the primitive members ($[La/Sm]_N$ = 1.0-1.3), which become LREE-enriched for the evolved ones ($[La/Sm]_N$ = 2.1-2.5). The Tafano Unit samples, on the other hand, are all LREE-enriched ($[La/Sm]_N$ = 3.0-4.7, respectively).

DISCUSSION

Petrogenetic constraints

Fractional crystallization

The analyzed rock samples collected from both units show wide ranges of SiO_2 contents. The compositional range in the Yerkuyu unit is actually significant (48.2-72.2 wt%) when the two evolved samples are considered (15-TF-8 and 15-TF-11). It is possible that the spread of SiO_2 resulted from alteration, because Si may be a relatively mobile element. However, SiO_2 appears to be somewhat correlated with Co, which is immobile, suggesting that Si is not extensively modified by alteration. In such a case, the wide range of SiO_2 would reflect the magmatic

diversity in both units, at least to some extent. Then, this would imply that fractional crystallization has played a significant role in the petrogenesis of the Tafano and Yerkuyu units.

The Mg, Co, Ni (also Cr) contents of the studied samples are all low. Indeed, even when the most primitive members of both units are considered, such elements invariably display low abundances when compared with the primary magmas, thus implying that they are also differentiated, possibly through mainly olivine as well as pyroxene fractionation. Considering this, and the compositional range shown by these elements, fractional crystallization was indeed significant for the petrogenesis of the studied samples, particularly for those from the Yerkuyu Unit. Another issue to be noted is that the two evolved samples from the Yerkuyu Unit suite appear as basaltic-andesitic/andesitic (based on the Nb/Y vs Zr/TiO_2 diagram) despite their very high SiO_2 contents (over 70 wt%). Since these samples (and all the others) display relative Nb deficiency (thus arc-like), they can also be tested using Co-Th diagram (Hastie et al., 2007). According to this plot (Fig 6), the two samples (15-TF-8 and 15-TF-11) are classified as dacite/rhyolite, which seems to fit better when the high silica content is considered.

In both units, Co and Ni decrease with increasing SiO_2 (Fig. 7a, b), suggesting fractionation of mafic phases, such as olivine and pyroxene. Plagioclase also appears to be a major fractionating phase, as evidenced by the decrease in Al_2O_3 with increasing SiO_2 (Fig. 7c). This is further supported by the negative correlation between CaO and SiO_2 (Fig. 7d). Such results are consistent with the observed phenocryst assemblage of olivine, pyroxene, and plagioclase in the Yerkuyu and Tafano Units. In terms of Fe_2O_3, two distinct trends emerge (Fig. 7e). The Yerkuyu Unit samples define a relatively flat trend first, which is followed then by a sharp decrease with increasing SiO_2. In contrast, the Tafano Unit samples display a continuous decrease towards more evolved compositions. The decrease in Fe_2O_3 in both groups may imply fractionation of Fe-Ti oxides. However, it seems that the saturation of Fe-Ti oxides probably occurs in the later stages for the Yerkuyu Unit, whereas they also dominate earlier stages for the Tafano Unit. The role of the Fe-Ti oxides is also reinforced with the similar behaviour of TiO_2 against SiO_2 for both groups (Fig. 7f). In addition, the effect of plagioclase and Fe-Ti oxide fractionation is dominant for the evolved sample from the Yerkuyu Unit (15-TF-8 and 15-TF-11), as displayed by the significant negative anomalies of Eu and Ti in the REE and multi-element patterns, respectively (Fig. 5).

Mantle source

To assess the mantle source characteristics, we largely concentrate on the relatively primitive samples to reduce the effect of fractional crystallization. Therefore, caution must be paid particularly for the two high-silica samples from the Yerkuyu Unit suite. The Zr-Nb element pair can be quite useful in the assessment of the mantle depletion/enrichment in the ancient igneous-derived rocks (e.g., Balci and Sayit, 2020). These elements display different incompatibilities; thus one can expect that they would be fractionated during melt extraction. Among the two, Nb has the higher incompatibility, therefore the melt extraction processes during the early crust-forming events in the Earth created relatively Nb-poor residual domains or reservoirs, which formed the depleted mantle (DM) (e.g., Hofmann, 1997) (also known as DMM - depleted MORB mantle). The depleted mantle, which is the typical source of N-MORBs, is therefore characterized by a high Zr/Nb ratio (34.2, Workman and Hart, 2005). In contrast, the Nb-rich, enriched domains/reservoirs are represented by lower Zr/Nb ratios (e.g., primitive mantle, Zr/Nb = 16.0; McDonough and Sun, 1995). The Yerkuyu Unit samples possess low Zr/Nb ratios (17.4-35.3), suggesting that they may have involved variable and substantial contribution from the DM component (Fig. 8a).

The Tafano Unit samples, on the other hand, display higher Zr/Nb ratios (10.1-15.6), which may imply a somewhat lower contribution from DM. This may, in turn, suggest a role for enriched sources in their petrogenesis. Also, it is possible that the relatively low Zr/Nb ratios can

result from low degrees of melting, considering that Zr and Nb have different incompatibilities. However, enriched components are regarded to have lower solidi and preferentially melt earlier with respect to the DM (which is characterized by dry, depleted peridotite) (e.g., Ito and Mahoney, 2005). Therefore, low-degree melts can be envisioned to mainly tap the readily fusible, enriched components rather than DM with higher solidus. This may, in turn, suggest that the enriched components may have been of greater importance for the petrogenesis of the Tafano Unit samples. The Nb/Yb ratio can further evaluate the rationality of this idea, in which two elements differ greatly in terms of partitioning during the melting of peridotitic upper mantle. With Nb being the more incompatible element in this pair, low Nb/Yb values particularly indicate the predominant involvement of DM (Nb/Yb = 0.4 for DMM; Workman and Hart, 2005). Among the two groups, the primitive Yerkuyu Unit samples display low Nb/Yb values (0.5-0.7), a feature also characteristic of N-MORBs thought to be derived from DM. Hence, the idea that the DM component is dominantly involved in the petrogenesis of the Yerkuyu Unit is also favoured by the Nb-Yb systematics. The higher Nb/Yb ratios of the Tafano Unit, on the other hand, support lesser involvement of DM, but more contribution from enriched sources.

All studied samples display marked and variable enrichment in LILE like Th and La relative to HFSE and HREE (Fig. 5). Such characteristics are typical of magmas generated at subduction-related settings (e.g., McCulloch and Gamble, 1991; Hawkesworth et al., 1993; Pearce and Peate, 1995). The decoupling between Th-La (and LILE) and HFSE-HREE is commonly attributed to the presence of some mineral phases in the subducting slab that strongly fractionate HFSE and HREE (e.g., sphene, rutile and garnet; Elliott et al., 1997; Class et al., 2000). Another alternative can be amphibole, which may be stable in the mnatle wedge and act as a sink for Nb and Ta (Ionov and Hoffman, 1995). Lastly, the low solubilities of HFSE are also considered in this regard, which may result in their fractionation especially from LILE (e.g., McCulloch and Gamble, 1991). Due to these reasons, Th, La, and LILE are not retained in the slab, and therefore, they are assumed to be subduction-mobile (Pearce and Stern, 2006). These elements are released via melt and/or fluids and they subsequently flux the mantle wedge, creating enrichment over HFSE and HREE. The analyzed samples, which are markedly enriched in these subduction-mobile elements, appear to have been derived from a mantle source metasomatized by slab-derived fluids/melts released during subduction.

The involvement of a subduction component is further supported by the plot of Nb/Yb vs Th/Yb (Pearce and Peate, 1995) (Fig. 8b). Nb and Yb are both strongly retained in the slab during the subduction processes (i.e., subduction-immobile); therefore, their addition to the mantle wedge is believed to be negligible (e.g., Pearce and Peate, 1995). Th, on the other hand, can be mobilized by sediment-derived melts, which, in turn, may metasomatize the mantle wedge (e.g,. Elliott et al., 1997). The net result of this process on the Th-Nb-Yb systematics is that the magmas derived from mantle sources with no subduction (i.e., MORBs and most OIBs) are distributed along an array, whereas any subduction addition will cause displacements from this array. In this plot (Fig. 8b), all analysed samples plot above the array, reinforcing the idea that variable subduction components have been added to their mantle sources.

Melt generation model

The LREE systematics of the studied samples vary between the tow groups and this reflects the combined effect of the slab-derived fluids/melt, degree of partial melting and nature of the source region. The HREE, on the other hand, are subduction-immobile, which makes them better indicators to understand the partial melting and mantle source mineralogy. Since HREE are strongly partitioned into the garnet, the presence of residual garnet in the mantle source would create fractionated HREE patterns (e.g., McKenzie and O'Nions, 1991). A garnet-free, spinel-bearing mantle source, however, would be characterized by flat HREE patterns with low Dy/Yb

ratios, owing to the low partition coefficients of HREE in spinel. All the Yerkuyu Unit samples and some from the Tafano Unit (IPS-13-59 and IPS-13-65) have relatively low Dy/Yb ratios, suggesting that they have derived dominantly from a spinel peridotite source. In contrast, the rest of the Tafano Unit samples shows relatively high Dy/Yb ratios compared to the others, which may imply the contribution of garnet-facies melts.

To test the involvement of spinel and/or garnet, and put some constraints on the nature of the source, we have performed a melt modeling (Fig. 9). The modeling employs a non-modal batch melting scheme and uses element ratios, thus minimizing the effects of fractionation crystallization. In addition, the considered elements are all subduction-immobile, so they are not modified by the slab-derived additions, which in turn enables us to understand better the melting process. Regarding the ratios used in the modeling, Nb/Yb is strongly sensitive to the degree of partial melting, since the large incompatibility difference between the two elements (e.g., Sun and McDonough, 1989). On the other hand, Dy/Yb, is sensitive to the presence of residual garnet due to the strong partitioning of HREE into garnet (e.g., Johnson, 1998). It must be kept in mind that partition coefficients strongly control the melt modeling; thus, the calculated melting arrays may differ based on the choice of partition coefficients. Further details regarding the modeling are given in Fig. 9.

The first thing to note about the melt modeling is that the samples from the Yerkuyu Unit do not appear to have involved garnet in their source region. A DM-type mantle that melts at spinel stability field can successfully reproduce compositions similar to the Yerkuyu Unit samples. On the other hand, in the Tafano Unit, where the variability in Dy/Yb is higher, although some samples are close to the spinel peridotite melting array, apparently this is not the case for most Tafano Unit samples. Therefore, for a first-order approximation, the modeling suggests that melting of spinel peridotite alone could not have produced the Tafano Unit samples. Thus, this also necessitates the involvement of garnet-facies melts.

As mentioned before, the Tafano Unit seems to have included a contribution from an enriched mantle sources. To put some constraints on this issue, we add an enriched source component as characterized by the C/FOZO-like melts from MORBs and OIBs. Wherever its ultimate origin is (e.g., lower mantle, transition zone; Hart et al., 1992), this recycled component can be thought to exist in the heterogeneous upper mantle as small pods or streaks enveloped by the DM-type mantle (e.g., Niu and Batiza, 1997). In our model, a Nb-enriched peridotite represents this component with modified E-DMM abundances (Sayit, 2013). In the model, the melting of this enriched peridotite is assumed to occur in the garnet-stability field. The calculated melting arrays suggest that the Tafano Unit samples is unlikely to be pure garnet-facies melts derived from this enriched component (Fig. 9). One alternative to this problem can be melt mixing, which involves melts generated at different depths of stability. In this solution, garnet-facies melts are assumed to be derived from the enriched component (which melts earlier and at greater depths), whereas the spinel-facies melts are sourced from the depleted component (which melts later and at shallower depths). The subsequent mixing of these melts appears to reproduce the compositions of the Tafano Unit samples (Fig. 9a). Another alternative would be the melting of pre-enriched mantle source, which has been fertilized by low-degree melts (before subduction addition). In this case, we assumed that the initial mantle source is characterized by depleted mantle, which is then metasomatized by the garnet-facies melts from the enriched component. Based on the modeling, the subsequent melting of this hybrid source can yield compositions like the Tafano Unit samples (Fig. 9b).

Tectonomagmatic characterization

All studied samples show subduction signatures (Figs. 5 and 8) suggesting their origin in a tectonic setting that most likely involves lithospheric subduction (either directly or indirectly) rather that mid-ocean ridge, oceanic island or oceanic plateau. The presence of subduction signatures, however, may have been acquired at several settings, including active or ancient subduction and some continental within-plate environments. To discriminate the possible tectonic setting(s) in which the studied samples from the Yerkuyu Unit have formed is so essential to discuss our data in the light of the different alternatives.

The acquisition of slab-derived fluids/melts derived from an ancient subduction event preserved in the sub-continental lithospheric mantle (SCLM) (e.g., Gibson et al., 1993) generally creates melt compositions with extreme trace element enrichment (e.g., Gibson et al., 1993). This feature is not documented in the analyzed samples, so we exclude this tectonic setting. At the same time continental within-plate origin does not seem plausible.

The active subduction case includes oceanic and continental arc-basin systems. The former is the simpler case. Since the continental lithosphere is not involved, oceanic arc-basin systems are generally more depleted than their continental counterparts and characterized by higher Zr/Nb, coupled with lower Nb/Yb ratios (e.g., Pearce and Peate, 1995). The Yerkuyu samples have these features suggesting an oceanic arc-basin tectonic setting. More in detail, the Yerkuyu samples show more depleted characteristics compared to the Tafano samples, suggesting that they are originated closest to an oceanic subduction system compared to those from the Tafano Unit (e.g., McCullough and Gamble, 1991; Pearce et al., 1995).

Arc-back arc pairs commonly characterize the oceanic subduction systems. The arcs are generally more depleted compared to the back arcs. This depletion is commonly attributed to the melt extraction at the back-arc region, which would yield a more depleted mantle that is subsequently tapped by the arc magmas (Woodhead et al., 1993). Considering the depletion levels, the Yerkuyu Unit suite is more likely to have been generated at an arc setting rather than back-arc.

On the contrary, the subduction-related characteristics and relatively enriched signatures of the Tafano Unit are typical of magmas generated at continental arcs in which melt generation largely takes place at the enriched continental lithospheric mantle with/without contamination by continental crust (e.g., Pearce, 1983). The involvement of continental lithosphere generally leads to lower Zr/Nb and higher Nb/Yb ratios as well as LREE enrichment. All these features fit well with the characteristics of Tafano Unit samples, suggesting their formation at a continental arc setting Ellero et al. (2015b).

The multi-element systematics support the reconstruction that the magmatic rocks of the Yerkuyu Unit and Tafano Unit were produced at oceanic arc and continental arc settings, respectively. The trace element patterns reveal that the Yerkuyu Unit shares similar characteristics with the oceanic arcs, such as Vanuatu (Fig. 10a) (Peate et al., 1997). In contrast, the Tafano Unit appears to be more akin to the continental arcs, such as Andes (Fig. 10b) (Bryant et al., 2006). The Th-Nb discrimination diagram of Saccani (2015) also provides a similar result (Fig. 10c).

The location of the magmatism within the Central Pontides: geodynamic implications

The geochemical features of the studied arc-type magmatic units suggest that during the Late Cretaceous the Central Pontides were characterized by two different geodynamic settings: an oceanic and a continental volcanic arc. According to the recent geodynamic reconstructions (e.g., Marroni et al., 2020), during the lower Late Cretaceous the IPS zone was already formed as the result of the convergent-related processes that produced the closure of the IPO basin and the subsequent collision between the SKT and IZT. At this time the IAEO basin was still open south of SKT and was characterized by a north-dipping subduction zone separated from the SKT

margin by a supra-subduction basin floored by a trapped oceanic crust (Bortolotti et al., 2018) (Fig. 11a). This crust was intruded since the upper Early Cretaceous by subduction-related magmatic rocks (Bortolotti et al., 2018). During the upper Late Cretaceous this supra-subduction basin was deformed as consequence of the processes that led the closure of the IAEO basin and incorporated to the suture zone located between SKT and TAM (Fig. 11b). During this stage, the subduction-related magmatism probably shifted from south to north (i.e., within the continental crust of SKT) (Fig. 11b).

The geodynamic significance of the arc-type magmatic units individuated in the Central Pontides (Yerkuyu Unit, Tafano Unit, and Kösdağ Unit) must be so interpreted considering this geodynamic reconstruction. Kösdağ and Yerkuyu units display oceanic arc-like geochemical characteristics. Having no direct information about the age of the Yerkuyu Unit, we can hypothesize that it is related to the same oceanic arc magmatism associated with the subduction of IAEO beneath the SKT which originates the Kösdağ Unit during the lower Late Cretaceous (Berber et al., 2021) (Fig. 11a). Kösdağ and Yerkuyu units are characterized by a different tectono-metamorphic evolution. The former shows low-grade metamorphism and a penetrative deformation (Berber et al., 2014; 2021) whereas Yerkuyu Unit is non-metamorphic and experienced only weak deformation. These features suggest an involvement of the Kösdağ Unit in the subduction zone, while Yerkuyu Unit appears to be accreted to the tectonic wedge at shallower structural levels without reaching significative subduction depth (Fig. 11b).

The Tafano Unit is instead characterized by geochemical signatures typical of a continental volcanic arc. It developed in the late Santonian-middle Campanian (Ellero et al., 2015b) simultaneously to the intrusion of the Beypazarı Granite (currently exposed NW of Ankara) into the SKT crust (Speciale et al., 2012; Helvacı et al., 2014). Consequently, it is possible to assume that the continental arc on the margin of the SKT developed only after the accretion of the oceanic volcanic arc in the tectonic wedge originated from the subduction of the IAE ocean (Fig. 11b).

After the closure of the IAEO basin, the IPS zone-SKT-IAES zone system was strongly modified by the strike-slip tectonics related with the activity of the NASZ constrained since the Early Eocene by Ottria et al. (2017). This tectonics dismembered the pre-existing flat-lying stack of tectonic units characterizing the tectonic wedges producing km-sized lozenge-shaped blocks bounded by sub-vertical strike-slip faults. Each of these blocks represents a fragment of tectonic unit translated of several tens of km along the NASZ and dislocated in a tectonic position completely different from that acquired before the Eocene.

CONCLUSIONS

Magmatic rocks collected from a fault-bounded block within the NASZ located to the west of Tosya (southern Central Pontides, Turkey) display a subduction-related geochemical signature that can be interpreted as originated from an intra-oceanic volcanic arc. This finding allowed to establish a new tectono-magmatic unit, the Yerkuyu Unit, which is characterized by a volcanic complex (basalts, basaltic andesites, basaltic dykes and sills, andesites and dacites) covered by discontinuous and thin calcarenite layers. Considering these stratigraphic features, the Yerkuyu Unit can be considered as the non-metamorphic equivalent of the Kösdağ Unit (Berber et al., 2021). Within the Late Cretaceous arc-type magmatic bodies of the southern Central Pontides, the comparison between the Yerkuyu Unit (this work), the Kösdağ Unit (Berber et al., 2014, 2021) and the Tafano Unit (Ellero et al., 2015b) indicates the existence of two diverse sites of magmatism: a continental arc located on the margin of the SKT for the Tafano Unit, and an intra-oceanic volcanic arc for the Yerkuyu Unit and the Kösdağ Unit. These results indicate a two-steps geodynamic evolution during the Late Cretaceous: i) the intra-oceanic subduction within IAEO yielded the Yerkuyu and Kösdağ units magmatism, and ii) the same descending slab beneath the thinned SKT continental lithosphere generated the Tafano Unit magmatism.

Moreover, this paper emphasizes that before to elaborate a complete geodynamic reconstruction in a region characterized by km-sized blocks bounded by strike-slip faults, it is mandatory to acquire detailed geological, petrographical, and geochemical features as well as time constraints for every single km-sized blocks.

ACKNOWLEDGEMENTS

This research was supported by the Darius Project, PRIN 2008 and PRIN 2010-11 projects (resp. M. Marroni) and PRA 2018 from University of Pisa. We thank the Prof. E. Piluso, an anonymous reviewer and Dr. M. Hässig for their careful and constructive review of the paper.

REFERENCES

Akbayram K., Okay A.I. and Satır M., 2013. Early Cretaceous closure of the Intra-Pontide Ocean in western Pontides (northwestern Turkey). J. Geod., 65: 38-55.

Altıner D., Koçyiğit A., Farinacci A., Nicosia U. and Conti M.A., 1991. Jurassic, Lower Cretaceous stratigraphy and paleogeographic evolution of the southern part of northwestern Anatolia. Geol. Rom., 28: 13-80.

Annen C., Scaillet B. and Sparks R.S.J., 2006. Thermal constraints on the emplacement rate of a large intrusive complex: the Manaslu Leucogranite, Nepal Himalaya. J. Petrol., 47 (1): 71-95.

Aydın M., Demir O., Özçelik Y., Terzioğlu N. and Satir M., 1995. A geological revision of Inebolu, Devrekani Agülı and Küre areas: new observations in PaleoTethys - NeoTethys sedimentary successions. In: A. Erler, T. Ercan, E. Bingöl and S. Örçen (Eds), Geology of the Black Sea Region. Maden Tetk. Arama Enst., Ankara, p. 33-38.

Aygül M. and Oberhansli R., 2017. Tectonic stacking of HP/LT metamorphic rocks in accretionary wedges and the role of shallowing slab-mantle decoupling. Tectonics, 36. https://doi.org/10.1002/2017TC004689.

Aygül M., Okay A.I., Oberhansli R., Schmidt A. and Sudo M., 2015. Late Cretaceous infant intra-oceanic arc volcanism, the Central Pontides, Turkey: petrogenetic and tectonic implications. J. Asian Earth Sci., 111: 312-327.

Aygül M., Okay A.I., Oberhänsli R. and Sudo M., 2016. Pre-collisional accretionary growth of the southern Laurasian margin, Central Pontides, Turkey. Tectonophysics, 671: 218-234.

Balci U. and Sayit K., 2020. Diabase dykes from Boğazkale (Çorum), Central Anatolia: Geochemical insights into the geodynamical evolution of the northern branch of Neotethys. Geochemistry, 80: 125602.

Berber F., Göncüoğlu M.C. and Sayit K., 2014. Geochemistry and tectonic significance of the Kösedağ metavolcanic rocks from the Sakarya Zone, Northern Turkey. In: Proceed. 20th CBGA Congr., Abstr., 1: 161-163, Tirana, Albania.

Berber F., Sayıt K. and Göncüoğlu M.C., 2021. Geochemistry and U-Pb ages from the Kösdağ Metavolcanics in southern Central Pontides (Turkey): Complementary data for early Late Cretaceous island arc development in the Northern Neotethys. Turk. J Earth Sci., 39: 51-80. doi: 10.3906/yer-2004-16.

Bortolotti V., Chiari M., Göncüoğlu M.C., Principi G., Saccani E., Tekin U.K. and Tassinari R., 2018. The Jurassic-Early Cretaceous basalt-chert association in the ophiolites of the Ankara Mélange, east of Ankara, Turkey: age and geochemistry. Geol. Mag., 155 (2): 451-478.

Bryant J.A., Yogodzinski G.M., Hall M.L., Lewicki. J.L. and Bailey D.G., 2006. Geochemical constraints on the origin of volcanic rocks from the Andean northern volcanic zone, Ecuador. J. Petrol., 47: 1147-1175.

Catanzariti R., Ellero A., Göncüoğlu M.C., Marroni M., Ottria G. and Pandolfi L., 2013. The Taraklı Flysch in the Boyalı area (Sakarya Terrane, Northern Turkey): Implications for the tectonic history of the Intrapontide Suture Zone. C.R. Geosci., 345: 454-461.

Class C., Miller D.M., Goldstein, S.L. and Langmuir C.H., 2000. Distinguishing melt and fluid subduction components in Umnak Volcanics, Aletuian Arc. Geoc. Geoph. Geos., 1, 1999GC000010.

Davidson J.P. and Tepley F.J., 1997. Recharge in volcanic systems: evidence from isotope profiles of phenocrysts. Science, 275: 826-829.

Derman S. and Sayılı A., 1995. Inaltı Formation: a keyunit for regional geology. In: Erler A., Ercan T., Bingöl, E. and Örçen S. (eds). Geology of the BlackSea Region. Proceedings of the International Sym-posium on the Geology of the Black Sea Region. Mineral Research and Exploration Institute of Turkey (MTA), 104-108.

Ellero A., Ottria G., Marroni M., Pandolfi L. and Göncüoglu M.C., 2015a. Analysis of the North Anatolian Shear Zone in Central Pontides (northern Turkey): Insight for geometries and kinematics of deformation structures in a transpressional zone. J. Struct. Geol., 72: 124-141.

Ellero A., Ottria G., Sayit K., Catanzariti R., Frassi C., Göncüoglu M.C., Marroni M. and Pandolfi L., 2015b. Geological and geochemical evidence for a Late Cretaceous continental arc in the Central Pontides, Northern Turkey. Ofioliti, 40: 73-90.

Elliott T., Plank T., Zindler A., White W. and Bourdon B., 1997. Element transport from slab to volcanic front at the Mariana arc. J. Geoph. Res., 102: 14991-15019.

Elmas A. and Yiğitbaş E., 2001. Ophiolite emplacement by strike-slip tectonics between the Pontide Zone and the Sakarya Zone in north-western Anatolia, Turkey. Intern. J. Earth Sci., 90: 257-269.

Eyüboglu Y., Santosh M., Dudas F.O., Akaryalı E., Chung S.L., Akdağ K. and Bektaş O., 2013. The nature of transition from adakitic to non-adakitic magmatism in a slab window setting: a synthesis from the eastern Pontides, NE Turkey. Geos. Frontiers, 4: 353-375.

Frassi C., Göncüoğlu M.C., Marroni M., Pandolfi L., Ruffini L., Ellero A., Ottria G. and Sayit K., 2016. The Intra-Pontide Suture Zone in the Tosya-Kastamonu area, Northern Turkey (with geological map at 1:50.000. J Maps, 12: 211-219.

Frassi C., Marroni M., Pandolfi L., Göncüoğlu, M.C., Ellero A., Ottria G., Sayit K., McDonald C.S., Balestrieri M.L. and Malasoma A., 2018. Burial and exhumation history of the Daday Unit (Central Pontides, Turkey): implications for the closure of the Intra-Pontide oceanic basin. Geol. Mag., 155: 356-376.

Frassi C., Rebay G., Marroni M., Sayit K., Göncüoğlu M.C., Ellero A., Ottria G. and Pandolfi L., 2020. Metamorphic imprint of ridge subduction on the Neo-Tethyan ophiolites from the Saka Unit (Central Pontides, northern Turkey). J. Asian Earth Sci., 200: 104468.

Gibson S.A., Thompson R.N., Leat P.T., Morrison M.A., Hendry G.L., Dickin A.P. and Mitchell J.G., 1993. Ultrapotassic magmas along the flanks of the Oligo-Miocene Rio Grande Rift, USA: Monitors of the zone of lithospheric mantle extension and thinning beneath a continental rift. J. Petrol., 34: 187-228.

Gill J.B., 1981. What is "Typical Calcalkaline Andesite"?. Orogenic andesites and plate tectonics. Springer, Berlin, Heidelberg, p. 1-12

Göncüoğlu M.C., 2019. A review of the geology and geodynamic evolution of tectonic terranes in Turkey. Min. Res. Turkey, p. 19-72.

Göncüoğlu M.C. and Erendil M., 1990. Pre-Late Cretaceous tectonic units of the Armutlu Peninsula. Proceed. of 8th Turkish Petroleum Congress, 8: 161-168.

Göncüoğlu M.C., Erendil M., Tekeli O., Aksay A., Kuşçu A. and Ürgün B., 1987. Geology of the Armutlu Peninsula. IGCP-5 Guide Book, 5: 12-18.

Göncüoglu M.C., Gürsu S., Tekin U.K. and Köksal S., 2008. New data on the evolution of the Neotethyan oceanic branches in Turkey: Late Jurassic ridge spreading in the Intra-Pontide branch. Ofioliti, 33: 153-164.

Göncüoglu M.C., Kozlu H. and Dirik K., 1997. Pre-Alpine and Alpine terranes in Turkey: explanatory notes to the terrane map of Turkey. Ann. Géol Pays Héllén., 37: 515-536.

Göncüoglu M.C., Marroni, M., Pandolfi L., Ellero A., Ottria G., Catanzariti R., Tekin U.K. and Sayit K., 2014. The Arkot Dağ Mélange in Araç area, central Turkey: Evidence of its origin within the geodynamic evolution of the Intra-Pontide suture zone. J. Asian Earth Sci., 85: 117-139.

Göncüoğlu M.C., Marroni M., Sayit K., Tekin U.K., Ottria G., Pandolfi L. and Ellero A., 2012. The Ayli Dağ ophiolite sequence (central-northern Turkey): A fragment of Middle Jurassic oceanic lithosphere within the Intra-Pontide suture zone. Ofioliti, 37: 77-91.

Göncüoğlu M.C., Sayit K. and Tekin U.K., 2010. Oceanization of the northern Neotethys: geochemical evidence from ophiolitic mélange basalts within the Izmir–Ankara suture belt, NW Turkey. Lithos, 116: 175–187.

Göncüoğlu M.C., Turhan N., Senturk K., Ozcan A. and Uysal S., 2000. A geotraverse across NW Turkey: tectonic units of the Central Sakarya region and their tectonic evolution. In: E. Bozkurt, J. Winchester and J.A. Piper (Eds.), Tectonics and magmatism in Turkey and the surrounding area. Geol. Soc. London, Spec. Publ., 173: 139-161.

Görür N., Monod O., Okay A.I., Sengör A.M.C., Tüysüz O., Yiğitbaş E., Sakinc M. and Akkök R., 1997. Palaeogeographic and tectonic position of the Carboniferous rocks of the western Pontides (Turkey) in the frame of the Variscan belt. Bull. Soc. Géol. Fr., 168: 197-205.

Hacker B.R., Kelemen P.B. and Behn M.D., 2015. Continental lower crust. Ann. Rev. Earth Planet. Sci., 43: 167-205.

Hart S.R., Hauri E.H. Oschmann L.A. and Whitehead J.A., 1992. Mantle plumes and entrainment: isotopic evidence. Science, 256: 517-520.

Hastie A.R., Kerr A.C., Pearce J.A. and Mitchell S.F., 2007. Classification of altered volcanic island arc rocks using immobile trace elements: development of the Th-Co discrimination diagram. J. Geol., 48: 2341-2357.

Hawkesworth C.J., Gallagher K., Hergt J.M. and McDermott F., 1993. Mantle and slab contributions in arc magmas. Ann. Rev. Earth Planet. Sci., 21: 175-204.

Helvacı C., Yücel Öztürk Y., Satır M. and Shang C.K., 2014. U-Pb zircon and K-Ar geochronology reveal the emplacement and cooling history of the Late Cretaceous Beypazarı granitoid, central Anatolia, Turkey. Intern. Geol. Rev., 56 (9): 1138-1155.

Hippolyte J.-C., Müller C., Kaymakçi N. and Sangu E., 2010. Dating of the Black Sea Basin: new nannoplankton ages from its inverted margin in the Central Pontides (Turkey). In: R.A. Stephenson, N. Kaymakci, M. Sosson, V. Starostenko and F. Bergerat (Eds.), Sedimentary basin tectonics from the Black Sea and Caucasus to the Arabian Platform. Geol. Soc. London, Spec. Publ., 340: 113-136. https://doi.org/10.1144/SP340.7

Hofmann A.W., 1997. Mantle geochemistry: The message from oceanic volcanism. Nature, 385: 219-229.

Humphris S.E. and Thompson G., 1978. Hydrothermal alteration of oceanic basalts by seawater. Geochimica et Cosmochimica Acta, 42: 107-125.

Johnson K.T., 1998. Experimental determination of partition coefficients for rare earth and high field-strength elements between clinopyroxene, garnet, and basaltic melt at high pressures. Contrib. Mineral. Petrol., 133: 60-68.

Ionov D. and Hoffman A.W., 1995. Nb-Ta-rich mantle amphiboles and micas: implications from subduction-related metasomatic trace element fractionations Earth Planet. Sci. Lett., 131: 341-356.

Ito G. and Mahoney J.J., 2005. Flow and melting of a heterogeneous mantle: 1. Method and importance to the geochemistry of ocean island and mid-ocean ridge basalts. Earth Planet. Sci. Lett., 230: 29-46.

Kent A.J., Darr C., Koleszar A.M., Salisbury M.J. and Cooper K.M., 2010. Preferential eruption of andesitic magmas through recharge filtering. Nature Geos., 3: 631-636.

Lee C.T.A. and Bachmann O., 2014. How important is the role of crystal fractionation in making intermediate magmas? Insights from Zr and P systematics. Earth Planet. Sci. Lett., 393: 266-274.

Marroni M., Frassi C., Göncüoglu M.C., Di Vincenzo G., Pandolfi L., Rebay G., Ellero A. and Ottria G.. 2014. Late Jurassic amphibolite-facies metamorphism in the Intra-Pontide Suture Zone (Turkey): an eastward extension of the Vardar Ocean from the Balkans into Anatolia? J. Geol. Soc., 171: 605-608.

Marroni M., Göncüoglu M.C., Frassi C, Sayit K., Pandolfi L., Ellero A. and Ottria G., 2020. The Intra-Pontide ophiolites in Northern Turkey revisited: from birth to death of a Neotethyan oceanic domain. Geos. Front., 11: 129-149.

McCulloch M.T. and Gamble J.A., 1991. Geochemical and geodynamical constraints on subduction zone magmatism. Earth Planet. Sci. Lett., 102: 358-374.

McDonough W.F. and Sun S.-S., 1995. The composition of the Earth. Chem. Geol., 120: 223-253.

McKenzie D. and O'Nions R.K., 1991. Partial melt distributions from inversion of rare earth element concentrations. J. Petrol., 32: 1021-1091.

Niu Y. and Batiza R., 1997. Trace element evidence from seamounts for recycled oceanic crust in the Eastern Pacific mantle. Earth Planet.Sci. Lett., 148: 471-483.

Okay A.I. and Topuz G., 2017. Variscan orogeny in the Black Sea region. Intern. J. Earth Sci., 106: 569-592.

Okay A.I. and Tüysüz O., 1999. Tethyan sutures of northern Turkey. In: B. Durand, L. Olivet, F. Horvath and M. Seranne (Eds.), Tethyan sutures of Northern Turkey. Geol. Soc. London Spec. Publ., 156: 475-515.

Okay A.I., Altıner D., Sunal G., Aygül M., Akdoğan R., Altiner S. and Simmons M., 2017. Geological evolution of the Central Pontides. In: M.D. Simmons, G. Tari and A.I. Okay (Eds.), Petroleum geology of the Black Sea. Geol. Soc., London Spec. Publ., 464. https://doi.org/10.1144/SP464.3.

Okay A.I., Satır M. and Siebel W., 2006. Pre-Alpide Palaeozoic and Mesozoic orogenic events in the Eastern Mediterranean region. In: Gee, D.G., Stepherson, R. A. (eds.), European Lithosphere Dynamics. Geol. Soc., London, Spec. Publ., 32: 389-06.

Okay A.I., Sunal G., Sherlock S., Altiner D., Tüysüz O., Kylander-Clark A.R. and Aygül M., 2013. Early Cretaceous sedimentation and orogeny on the active margin of Eurasia: Southern Central Pontides, Turkey. Tectonics, 32 (5):1247-1271.

Okay A.I., Sunal G., Sherlock S., Kylander-Clark A.R. and Özcan E., 2020. İzmir-Ankara Suture as a Triassic to Cretaceous Plate Boundary- Data from Central Anatolia. Tectonics, 39 (5): e2019TC005849.

Okay A.I., Sunal G., Tüysüz O., Sherlock S., Keskin M. and Kylander-Clark A.R.C., 2014. Low-pressure-high temperature metamorphism during extension in a Jurassic magmatic arc, Central Pontides, Turkey. J. Metam. Geol., 32: 49-69.

Okuyucu C., Dimitrova T.K., Göncüoğlu M.C. and Gedik I., 2017. Late Permian (Tatarian) fluvio-lacustrine successions in NW Anatolia (Zonguldak Terrane, Turkey): palaeogeographic implications. Geol. Mag., 154: 1073-1087.

Ottria G., Pandolfi L., Catanzariti R., Da Prato S., Ellero A., Frassi C. and Göncüoğlu M.C., 2017. Evolution of an Early Eocene pull-apart basin in the Central Pontides (Northern Turkey): new insights into the origin of the North Anatolian Shear Zone. Terra Nova, 29: 392-400.

Özcan E., Less G. and Kertesz B., 2007. Late Ypresian to middle Lutetian Orthophragminid record from central and northern Turkey: Taxonomy and remarks on zonal scheme. Turk. J. Earth Sci., 16: 281-318.

Pearce J.A., 1983. Role of the sub-continental lithosphere in magma genesis at active continental margins. In: C.J. Hawkesworth and M.J. Norry (Eds.), Continental basalts and mantle xenoliths. Shiva Press, Nantwich, U.K., p. 230-249.

Pearce J.A. and Peate D.W., 1995. Tectonic implications of the composition of volcanic arc magmas. Ann. Rev. Earth Planet. Sci., 23: 251-285.

Pearce J.A. and Stern R.J., 2006. Origin of back-arc basin magmas: trace element and isotope perspectives. Geophys. Monogr. Am. Geophys. Union, 166: 63.

Pearce J.A., Baker P.E., Harvey P.K. and Luff I.W., 1995. Geochemical evidence for subduction fluxes, mantle melting and fractional crystallization beneath the South Sandwich island arc. J. Petrol., 36 (4): 1073-1109.

Peate D.W., Pearce J.A., Hawkesworth C.J., Colley H., Edwards C.M.H. and Hirose K., 1997. Geochemical variations in Vanuatu arc lavas: the role of subducted material and a variable mantle wedge composition. J. Petrol., 38:1331-1358.

Plank T. and Langmuir C.H., 1988. An evaluation of the global variations in the major element chemistry of arc basalts. Earth Planet. Sci. Lett., 90 (4): 349-370.

Reubi O. and Blundy J., 2009. A dearth of intermediate melts at subduction zone volcanoes and the petrogenesis of arc andesites. Nature, 461 (7268): 1269-1273.

Rice S.P., Robertson A.H. and Ustaömer T., 2006. Late Cretaceous-Early Cenozoic tectonic evolution of the Eurasian active margin in the Central and Eastern Pontides, northern Turkey. In: Geol. Soc., London Spec. Publ., 260 (1): 413-445.

Ringwood A.E., 1974. The petrological evolution of island arc systems: Twenty-seventh William Smith Lecture. J Geol. Soc., 130 (3): 183-204.

Robertson A., Parlak O., Ustaömer T., Taslı K., Inan N., Dumitrica P. and Karaoglan F., 2013. Subduction, ophiolite genesis and collision history of Tethys adjacent to the Eurasian continental margin: new evidence from the Eastern Pontides, Turkey. Geod. Acta, 26: 230-293.

Robertson A.H.F. and Ustaömer T., 2004. Tectonic evolution of the Intra-Pontide suture zone in the Armutlu Peninsula, NW Turkey. Tectonophysics, 381: 175-209.

Saccani E., 2015. A new method of discriminating different types of post-Archean ophiolitic basalts and their tectonic significance using Th-Nb and Ce-Dy-Yb systematics. Geos. Front., 6: 481-501.

Sayit K., 2013. Immobile trace element systematics of ocean island basalts: the role of oceanic lithosphere in creating the geochemical diversity. Ofioliti, 38 (1): 101-120.

Sayit K., Bedi Y., Tekin U.K., Göncüoğlu M.C. and Okuyucu C., 2017. Middle Triassic back-arc basalts from the blocks in the Mersin Mélange, southern Turkey: Implications for the geodynamic evolution of the Northern Neotethys. Lithos, 268-271: 102-113.

Sayit K., Marroni M., Göncüoğlu M.C., Pandolfi L., Ellero A., Ottria G. and Frassi C., 2016 Geological setting and geochemical signatures of the mafic rocks from the Intra-Pontide Suture Zone: Implications for the geodynamic reconstruction of the Mesozoic Neotethys. Intern. J. Earth Sci., 105 (1): 39-64.

Şengör A.M.C. and Yilmaz Y., 1981. Tethyan evolution of Turkey, a plate tectonic approach. Tectonophysics, 75: 181-241.

Şengör A.M.C., Tüysüz O., Imren C., Sakınç M., Eyidoğan H., Görür N., Le Pichon X. and Rangin C., 2005. The North Anatolian fault: A new look. Ann. Rev. Earth Planet. Sci., 33: 37-112.

Speciale P.A., Catlos E.J., Yıldız G.O., Shin T.A. and Black K.N., 2012. Zircon ages from the Beypazarı granitoid pluton (north central Turkey): tectonic implications. Geod. Acta, 25 (3-4): 162-182.

Staudigel H., Plank T., White B. and Schmincke H-U., 1996. Geochemical fluxes during seafloor alteration of the basaltic upper oceanic crust: DSDP sites 417 and 418. AGU Geophys. Monogr., 96: 19-38.

Stern C.R., 1991. Comment on "Crustal contributions to arc magmatism in the Andes of Central Chile" by W. Hildreth and S. Moorbath. Contr. Miner. Petrol., 108, 1-2: 241-246.

Stern C.R., 2011. Subduction erosion: rates, mechanisms, and its role in arc magmatism and the evolution of the continental crust and mantle. Gondw. Res., 20: 284-308.

Stern S., Cimarelli C., Gaudin D., Scheu B. and Dingwell D.B., 2019. Dataset for the influence of water content and temperature on electrification in rapid decompression experiments. GFZ Data Services.

Straub S.M., Gómez-Tuena A. and Vannucchi P., 2020. Subduction erosion and arc volcanism. Nat. Rev. Earth & Envir., 1 (11): 574-589.

Streck M.J., Leeman W.P. and Chesley J., 2007. High-magnesian andesite from Mount Shasta: A product of magma mixing and contamination, not a primitive mantle melt. Geology, 35 (4): 351-354.

Sun S.-S. and McDonough W.F., 1989. Chemical and isotopic systematics of oceanic basalts: implications for mantle composition and processes. In: A.D. Saunders and M.J. Norry (Eds.), Geol. Soc. London, Spec. Publ., 42: 313-345.

Tekin U.K., Göncüoğlu M.C., Pandolfi L. and Marroni M., 2012. Middle-Late Trias radiolarian cherts from the Arkotdağ mélange in northern Turkey: implications for the life span of the northern Neotethyan branch. Geodyn. Acta, 25 (3-4): 305-319.

Tekin U.K., Okuyucu C., Sayit K., Bedi Y., Noble P.J., Krystyn L. and Göncüoğlu M.C., 2019. Integrated radiolaria, benthic foraminifera and conodont biochronology of the pelagic Permian blocks/tectonic slices and geochemistry of associated volcanic rocks from the Mersin Mélange, southern Turkey: Implications for the Permian evolution of the northern Neotethys. Isl. Arc, 28: 1-36.

Tüysüz O., 1990. Tectonic evolution of a part of the Tethyside orogenic collage: The Kargı Massif, northern Turkey. Tectonics, 9: 141-160.

Tüysüz O., 1999. Geology of the cretaceous sedimentary basins of the western Pontides. Geol.l J., 34: 75–93.

Tüysüz O. and Yiğitbaş E., 1994. The Karakaya basin: A Palaeo-Tethyan marginal basin and its age of opening. Acta Geol. Hung., 37: 327-350.

Tüysüz O., Dellaloğlu A.A. and Terzioğlu N., 1995. A magmatic belt within the Neo-Tethyan suture zone and its role in the tectonic evolution of northern Turkey. Tectonophysics, 243 (1-2): 173-191.

Ustaömer T. and Robertson A.H.F., 1999. Geochemical evidence used to test alternative plate tectonic models for the pre-Upper Jurassic (Palaeotethyan) units in the Central Pontides, N Turkey. Geol. J., 34: 25-53.

Winchester J.A. and Floyd P.A., 1977. Geochemical discrimination of different magma series and their differentiation products using immobile elements. Chem. Geol., 20: 325-343.

Woodhead J., Eggins S. and Gamble J., 1993. High field strength and transition element systematics in island arc and back-arc basin basalts: evidence for multi-phase melt extraction and a depleted mantle wedge. Earth Planet. Sci. Lett., 114: 491-504.

Workman R.K. and Hart S.R., 2005. Major and trace element composition of the depleted MORB mantle (DMM). Earth Planet. Sci. Lett., 231: 53-72.

Yalınız M.K., Floyd P.A. and Göncüoğlu M.C., 1996. Supra-subduction zone ophiolites of Central Anatolia: geochemical evidence from the Sarıkaraman Ophiolite, Aksaray, Turkey. Miner. Mag., 60: 697-710.

Yılmaz Y. 1990. Allochthonous terranes in the Tethyan Middle East, Anatolia and surrounding regions. Philos. Trans. Royal Soc. London, A, 331: 611-624

Yılmaz Y., Tüysüz O., Yiğitbaş E., Genç S.C. and Şengör A.M.C., 1997. Geology and tectonic evolution of the Pontides. In: A.G. Robinson (Ed.), Regional and petroleum geology of the Black Sea and surrounding region. Bull. Am. Ass. Petrol. Geol., 68: 183-226

Figure captions

Fig. 1 - Tectonic sketch map of the Anatolian Peninsula and location of the study area (modified after Okay and Tüysüz, 1999).

Fig. 2 - Geological sketch map of the Central Pontides (compiled from Okay et al., 2006; 2014; Hippolyte et al., 2010; Göncüoğlu et al., 2012; Marroni et al., 2014; Ellero et al., 2015a; 2015b; Frassi et al., 2016; 2018; Sayit et al., 2017).

Fig. 3 - The Tafano and the Yerkuyu units. (a) Photomicrograph of a porphyritic basaltic andesite from the Tafano Unit, with clinopyroxene and altered plagioclase phenocrysts (Cross-polarized light). (b) Basalt-breccia interlayered with andesites of the Basal Volcanic Complex within the Tafano Unit. (c) Basalt from the Yerkuyu Unit. (d) Calcarenite layers covering the Basal Volcanic Complex in the Yurkuyu Unit. (e) Photomicrograph of porphyritic dacite from the Yerkuyu Unit, with polysynthetically twinned plagioclase and corroded quartz phenocrysts embedded in a fine-grained groundmass (Cross-polarized light). (f) Photomicrograph of porphyritic andesite from the Yerkuyu Unit, with large, zoned plagioclase phenocrysts (Plane-polarized light).

Fig. 4 - Chemical classification of the igneous lithologies from the Tafano and Yerkuyu units (after Winchester and Floyd, 1977). The Tafano Unit data from Ellero et al. (2015b).

Fig. 5 - Multi-element and REE patterns of the igneous lithologies from the Tafano and Yerkuyu units. Normalization values from Sun and McDonough (1989). The Tafano Unit data from Ellero et al. (2015b).

Fig. 6 - Classification of the Tafano and Yerkuyu lithologies on the basis of Th-Co systematics (after Hastie et al., 2007). IAT- Island Arc Tholeiite; CA- Calc-alkaline; H-K and Sh-: High-K and Shoshonite; Basalt, B/A- Basalt/Andesite; D/R- Dacite/Rhyolite. The Tafano Unit data from Ellero et al. (2015b).

Fig. 7 - Binary variation plots of selected major and trace elements against SiO_2 for the assessment of fractional crystallization. The Tafano Unit data from Ellero et al. (2015b).

Fig. 8 - Zr/Nb vs Nb/Yb and Nb/Yb vs Th/Yb plots to understand the nature of the mantle source and subduction contribution. The Tafano Unit data from Ellero et al. (2015b).

Fig. 9 - Melt modeling of the basaltic/andesitic lithologies from the Tafano and Yurkuyu units. Regarding spinel-peridotite melting, the mantle source is assumed to be of DMM composition (Workman and Hart, 2005), in which the mode was taken as 0.612 ol + 0.203 opx + 0.135 cpx + 0.025 sp, which melts in the proportions 0.02 ol + 0.08 opx + 0.75 cpx + 0.15 sp. The garnet-peridotite source, on the other hand, is of E-DMM composition (Workman and Hart, 2005) with the exception of Nb, which is assumed to be 0.35 ppm (Sayit, 2013). The mode of this source was assumed to be 0.60 ol + 0.20 opx + 0.14 cpx + 0.06 grt (McKenzie and O'Nions, 1991), which melts in the proportions of 0.01 ol + 0.04 opx + 0.55 cpx + 0.04 grt. Straight lines in the figure (a) are mixing lines constructed between garnet-facies and spinel-facies melts, where tick marks were drawn to represent 10% intervals. In (b), the enriched metasomatized source (before subduction addition) is produced by 3% addition of modified E-DMM garnet-facies melt (F = 0.01%) to DMM-type peridotite. The source and melt modes of this metasomatized garnet peridotite are assumed to be the same as in the E-DMM garnet peridotite. The Tafano Unit data from Ellero et al. (2015b).

Fig. 10 - Tectonomagmatic characterization of the Tafano and Yurkuyu igneous lithologies using (a, b) multielement patterns. The Tafano Unit data from Ellero et al. (2015b). Vanuatu Arc sample is MLM7; Peate et al. (1997); whereas Andes Northern Volcanic Zone sample is HHV; Bryant et al. (2006); using (c) Th-Nb systematics of Saccani (2015).

Fig. 11 - Two-dimensional geodynamic reconstruction for the Late Cretaceous volcanic arc units of the southern Central Pontides (not to scale). K- Kösdağ Unit; Y- Yerkuyu Unit; T-Tafano Unit; TAM- Tauride Anatolide Microplate; IAEO- Izmir-Ankara-Erzincan Ocean; SKT- Sakarya Terrane; IPS- Intra Pontide Suture zone; IZT- Istanbul-Zonguldak Terrane.

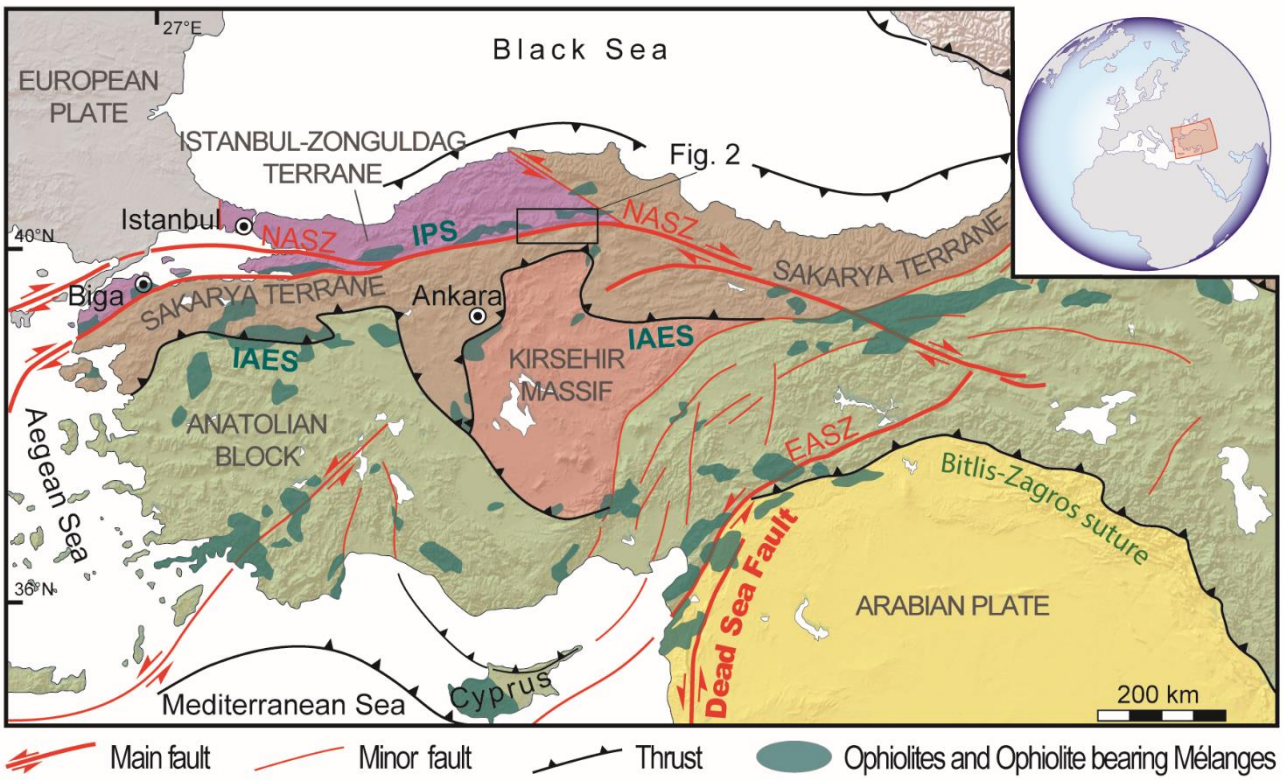
27°E
Black Sea
EUROPEAN PLATE
ISTANBUL-ZONGULDAG TERRANE
Fig. 2
Istanbul
NASZ
IPS
NASZ
40°N
SAKARYA TERRANE
Biga
SAKARYA TERRANE
Ankara
IAES
IAES
KIRSEHIR MASSIF
ANATOLIAN BLOCK
Aegean Sea
EASZ
Bitlis-Zagros suture
Dead Sea Fault
ARABIAN PLATE
36°N
Mediterranean Sea
Cyprus
200 km
Main fault
Minor fault
Thrust
Ophiolites and Ophiolite bearing Mélanges

Fig. 1

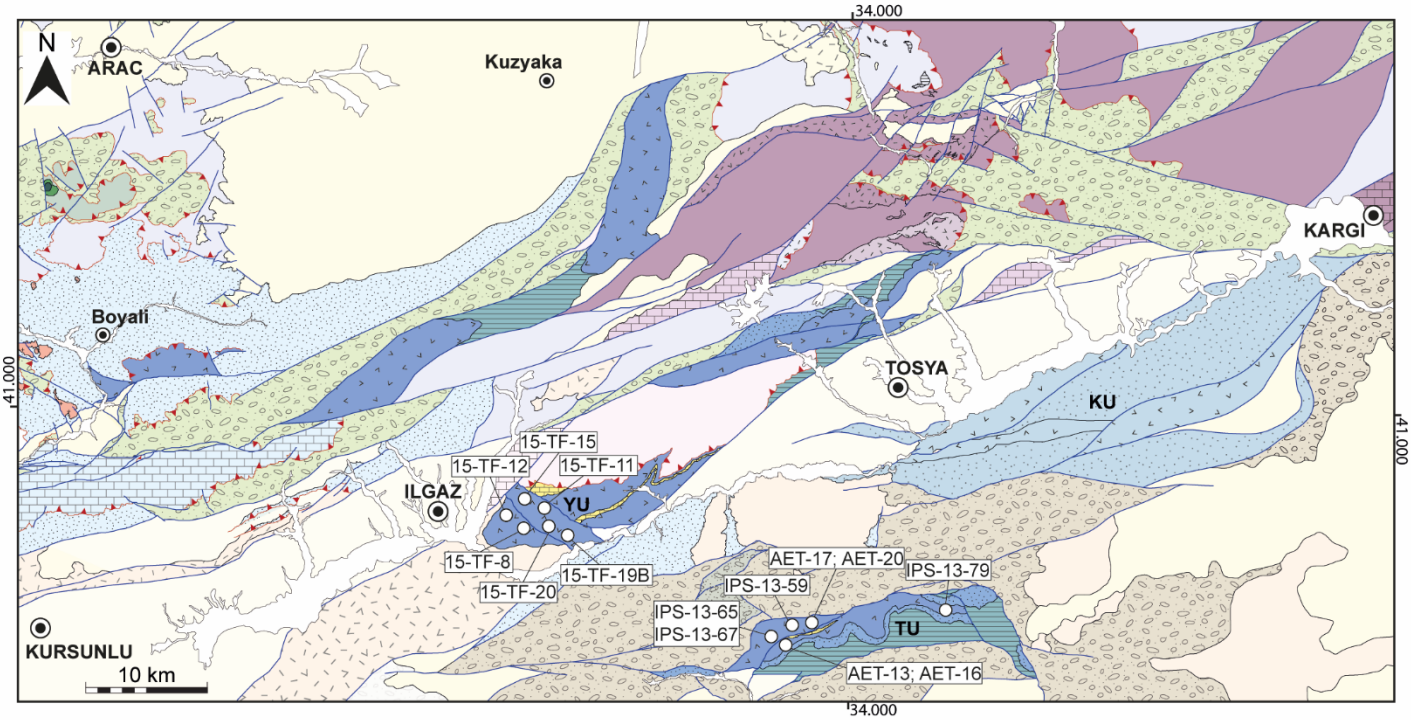

Quaternary Alluvial Deposits

Pliocene Sedimentary Deposits

Miocene Volcanites

Miocene Sedimentary Deposits

Eocene Volcanites

Eocene Sedimentary Deposits

LATE CRETACEOUS VOLCANIC ARC UNITS

Metamorphic Unit (Kösdağ Unit KU)

Sedimentary cover succession

Volcanic rocks

Non-Metamorphic Units (Tafano Unit TU, Yerkuyu Unit YU)

Marly-Calcareous Turbidite Formation

Volcaniclastic Sandstone Formation

Calcarenites and Calcirudites

Basal Volcanic Complex

SAKARYA TERRANE

Tarakli Flysch (Early Maastrichtian - Middle Paleocene)

Limestones (Late Jurassic - Early Cretaceous)

INTRA-PONTIDE SUTURE ZONE

Middle Jurassic Granites

Central Pontides Structural Complex

Ayli Dağ ophiolite Unit. a) Serpentinite; b) Gabbro; c) Basalt. (Bathonian-early Callovian)

Arkot Dağ mèlange (Late Santonian)

Emirköy Unit. a) Metapelites; b) Metalimestones. (? Cretaceous)

Daday Unit. a) Micaschists; b) Metabasites. (?Late Triassic - ?Early Jurassic)

Saka Unit (?Late Triassic - ?Early Jurassic)

Domuz Dağ Unit. a) Micaschists; b) Amphibolites; c) Metalimestones. (?Late Triassic - ?Early Jurassic)

IZMIR-ANKARA-ERZINCAN SUTURE ZONE

Ophiolitic Mèlange

SYMBOLS

Stratigraphic Boundaries

Thrusts Surfaces

Faults

Sample

Fig. 2

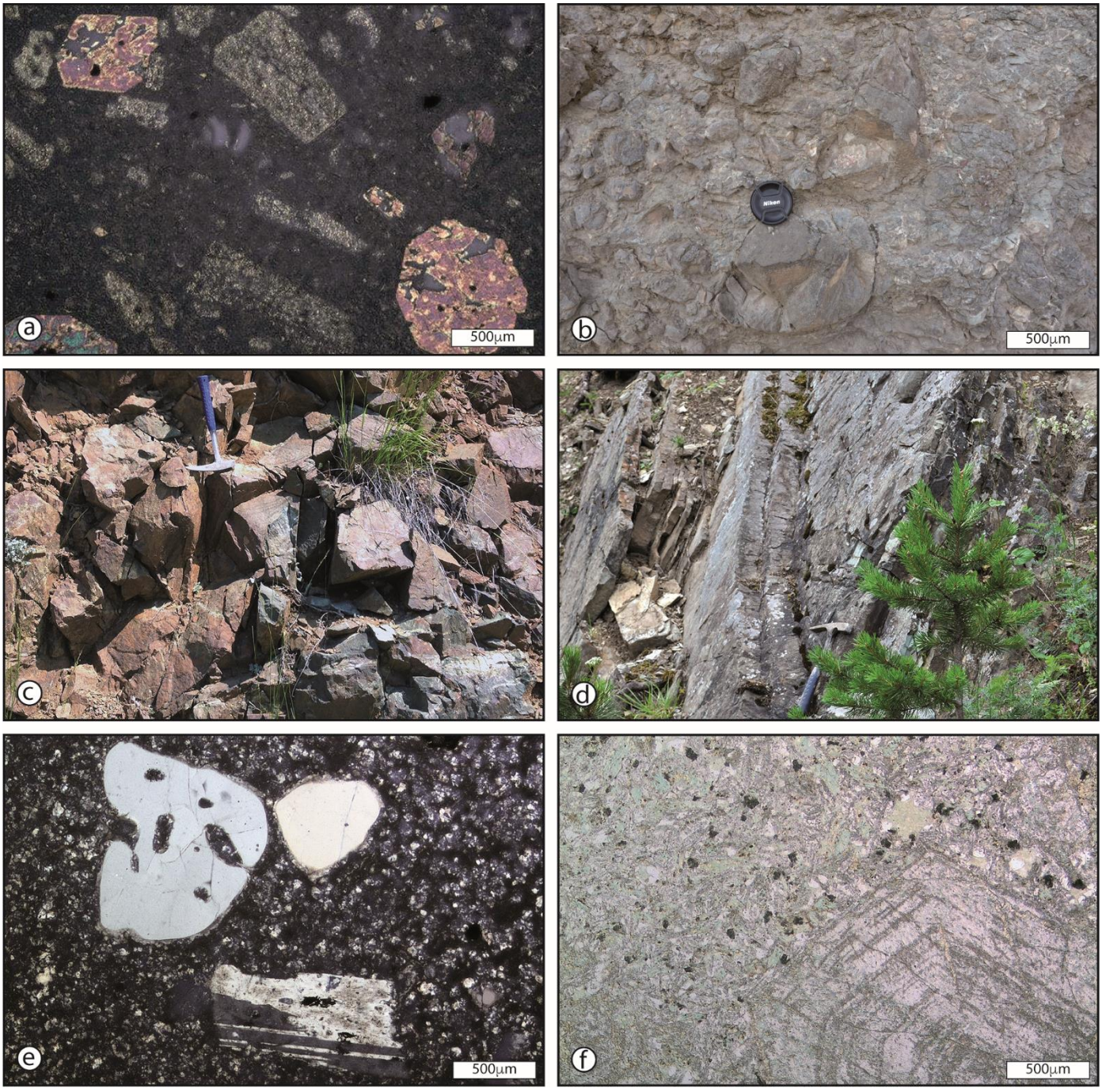

Fig. 3

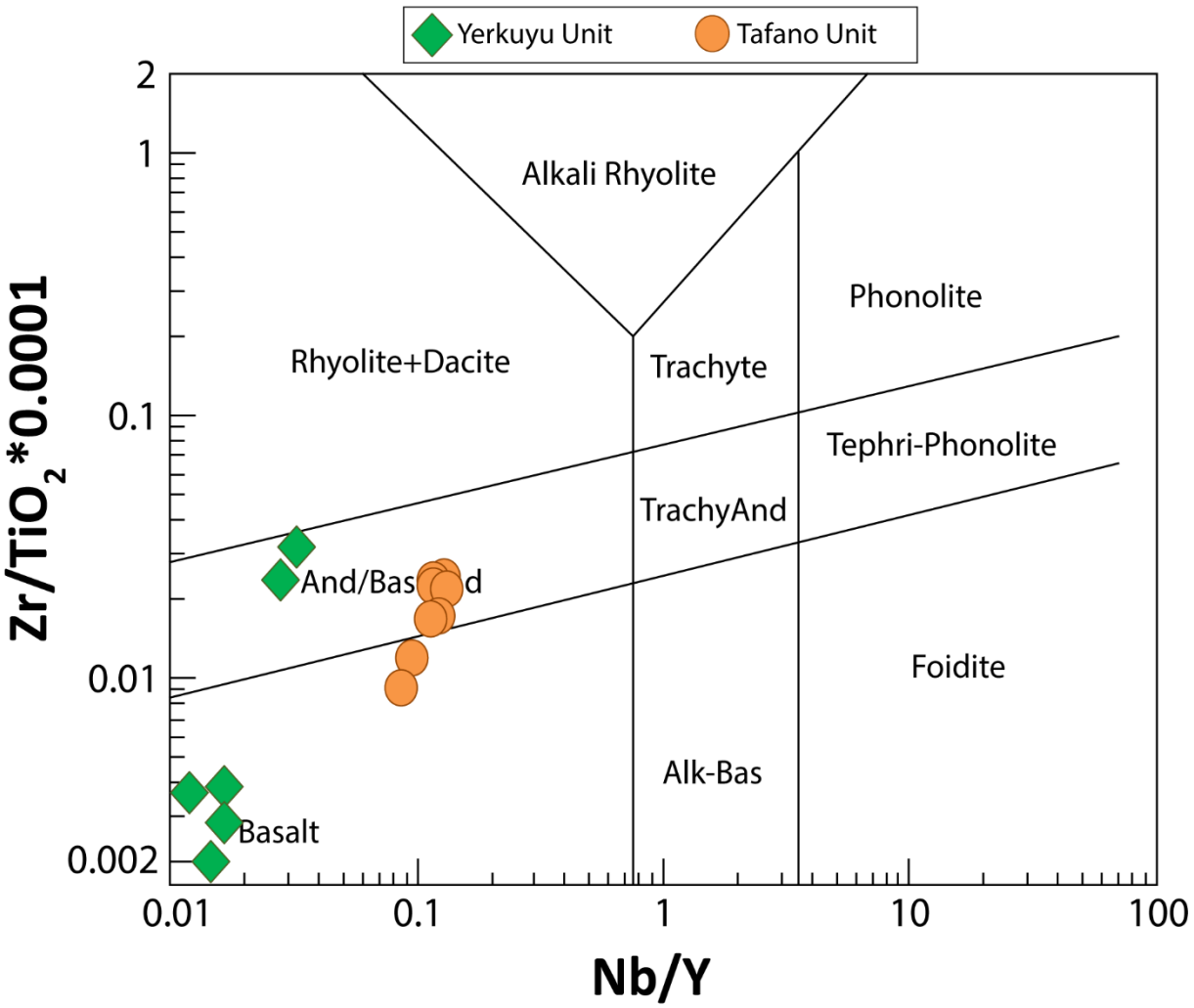
Yerkuyu Unit
Tafano Unit
Alkali Rhyolite
Phonolite
Rhyolite+Dacite
Trachyte
Tephri-Phonolite
TrachyAnd
And/Bas d
Foidite
Alk-Bas
Basalt
2
1
0.1
0.01
0.002
0.01
0.1
1
10
100
Zr/TiO2*0.0001
Nb/Y

Fig. 4

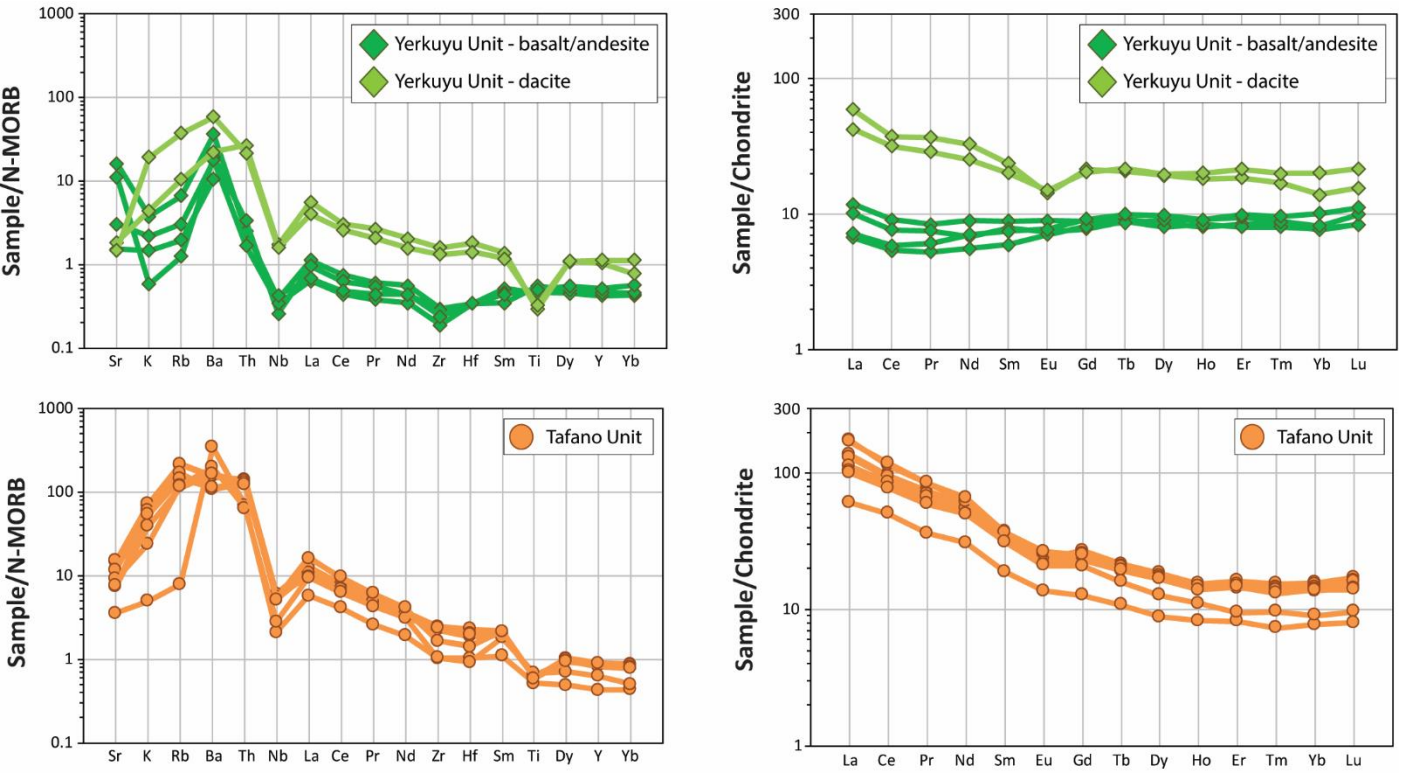
Sample/N-MORB
1000
100
10
1
0.1
Yerkuyu Unit - basalt/andesite
Yerkuyu Unit - dacite
Sr K Rb Ba Th Nb La Ce Pr Nd Zr Hf Sm Ti Dy Y Yb
Sample/Chondrite
300
100
10
1
Yerkuyu Unit - basalt/andesite
Yerkuyu Unit - dacite
La Ce Pr Nd Sm Eu Gd Tb Dy Ho Er Tm Yb Lu
Sample/N-MORB
1000
100
10
1
0.1
Tafano Unit
Sr K Rb Ba Th Nb La Ce Pr Nd Zr Hf Sm Ti Dy Y Yb
Sample/Chondrite
300
100
10
1
Tafano Unit
La Ce Pr Nd Sm Eu Gd Tb Dy Ho Er Tm Yb Lu

Fig. 5

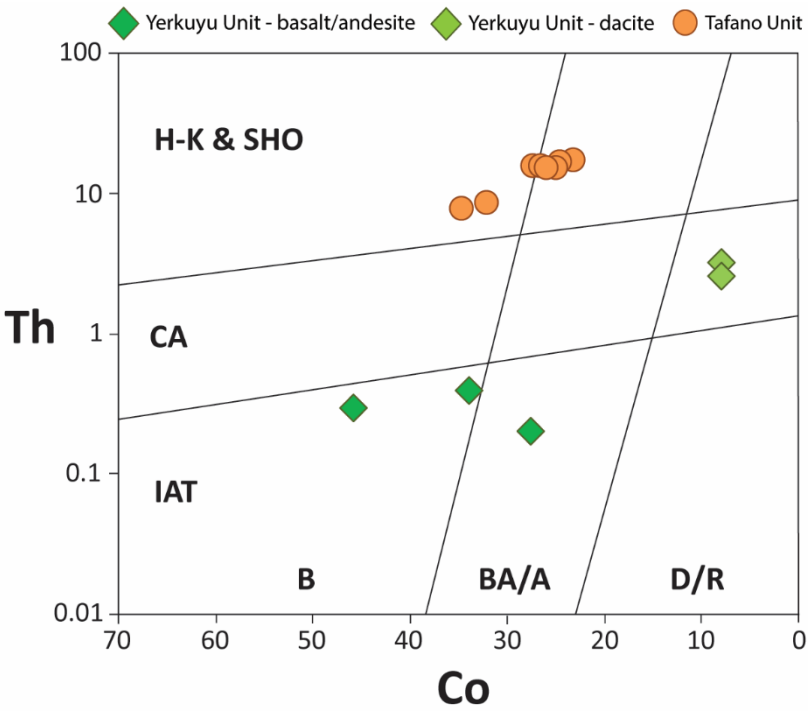
Yerkuyu Unit - basalt/andesite
Yerkuyu Unit - dacite
Tafano Unit
100
10
1
0.1
0.01
Th
H-K & SHO
CA
IAT
B
BA/A
D/R
70
60
50
40
30
20
10
0
Co

Fig. 6

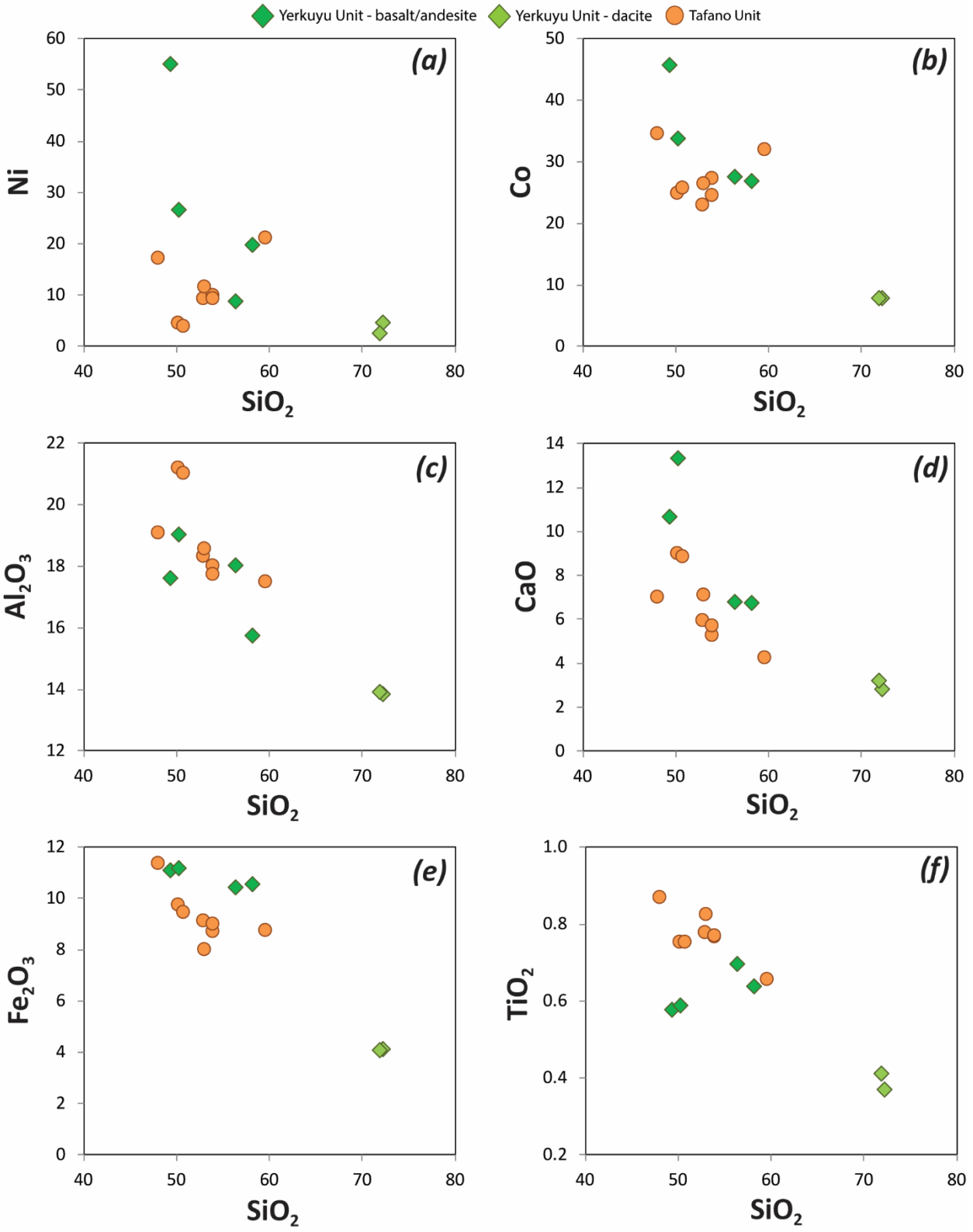
Yerkuyu Unit - basalt/andesite
Yerkuyu Unit - dacite
Tafano Unit
(a)
Ni
SiO2
(b)
Co
SiO2
(c)
Al2O3
SiO2
(d)
CaO
SiO2
(e)
Fe2O3
SiO2
(f)
TiO2
SiO2

Fig. 7

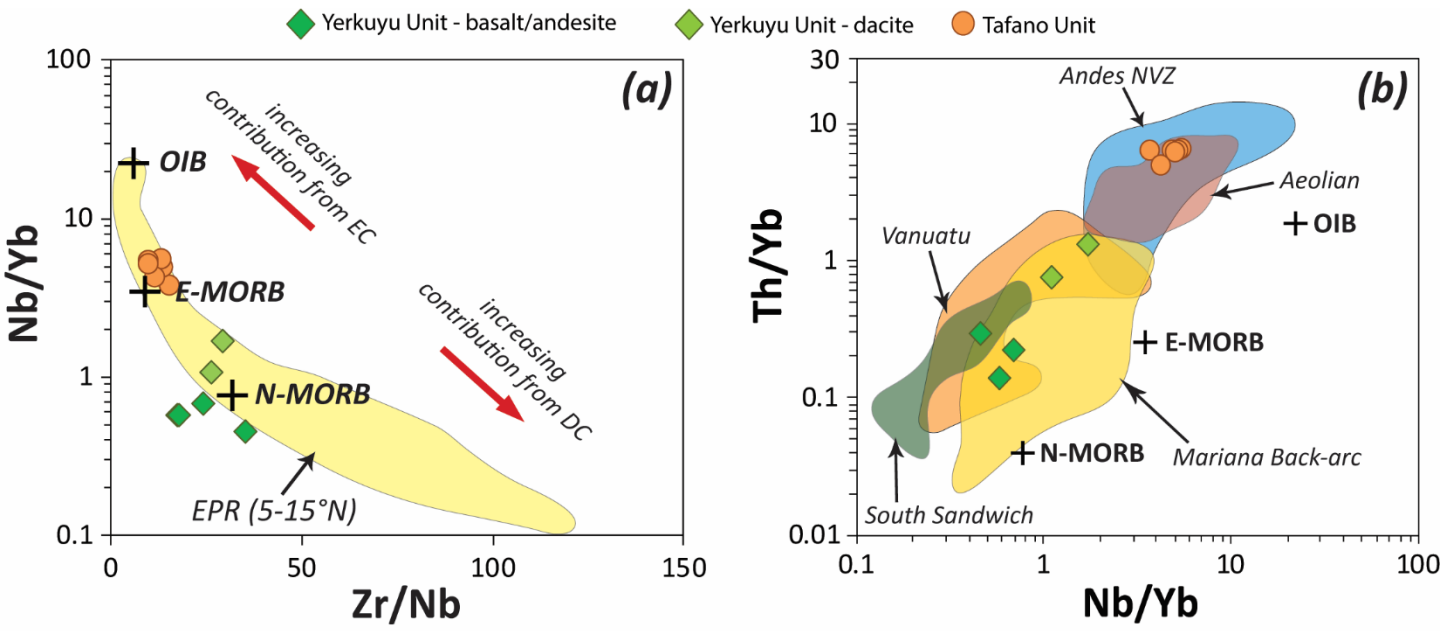
Yerkuyu Unit - basalt/andesite
Yerkuyu Unit - dacite
Tafano Unit
(a)
OIB
E-MORB
N-MORB
increasing contribution from EC
increasing contribution from DC
EPR (5-15°N)
Nb/Yb
Zr/Nb
100
10
1
0.1
0
50
100
150
(b)
Andes NVZ
Aeolian
OIB
Vanuatu
E-MORB
N-MORB
Mariana Back-arc
South Sandwich
Th/Yb
Nb/Yb
30
10
1
0.1
0.01
0.1
1
10
100

Fig. 8

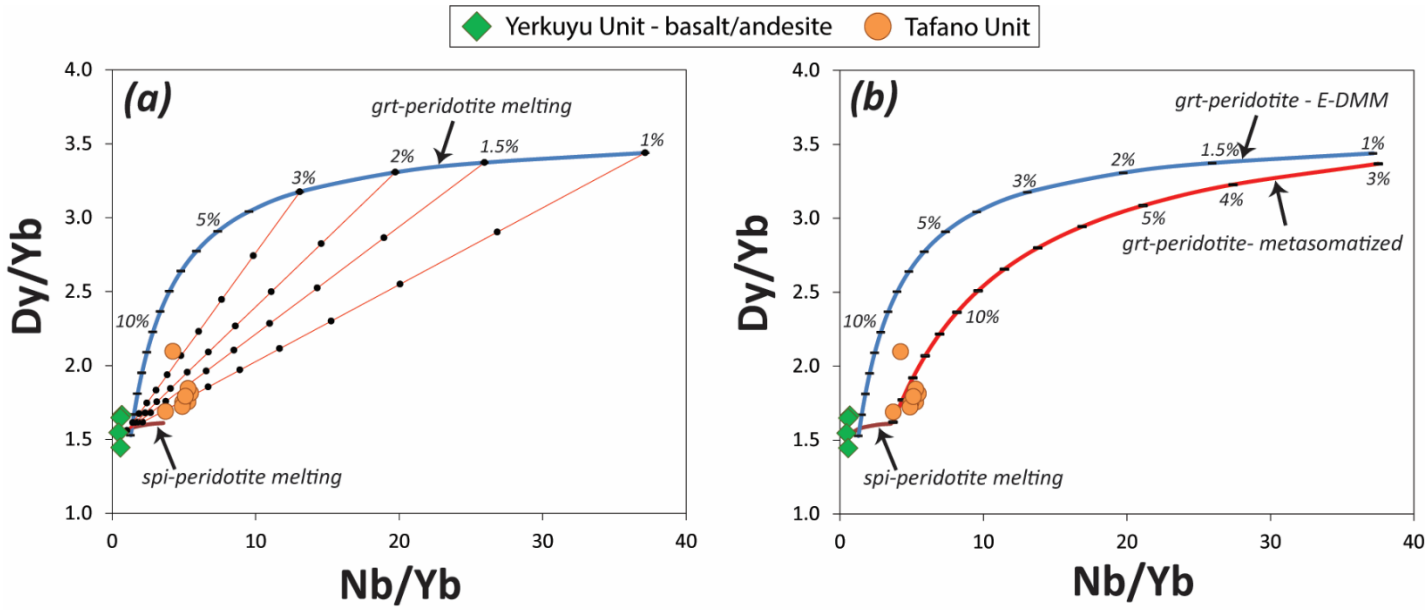
Yerkuyu Unit - basalt/andesite
Tafano Unit
(a)
grt-peridotite melting
spi-peridotite melting
1%
1.5%
2%
3%
5%
10%
Dy/Yb
Nb/Yb
(b)
grt-peridotite - E-DMM
grt-peridotite- metasomatized
4%

Fig. 9

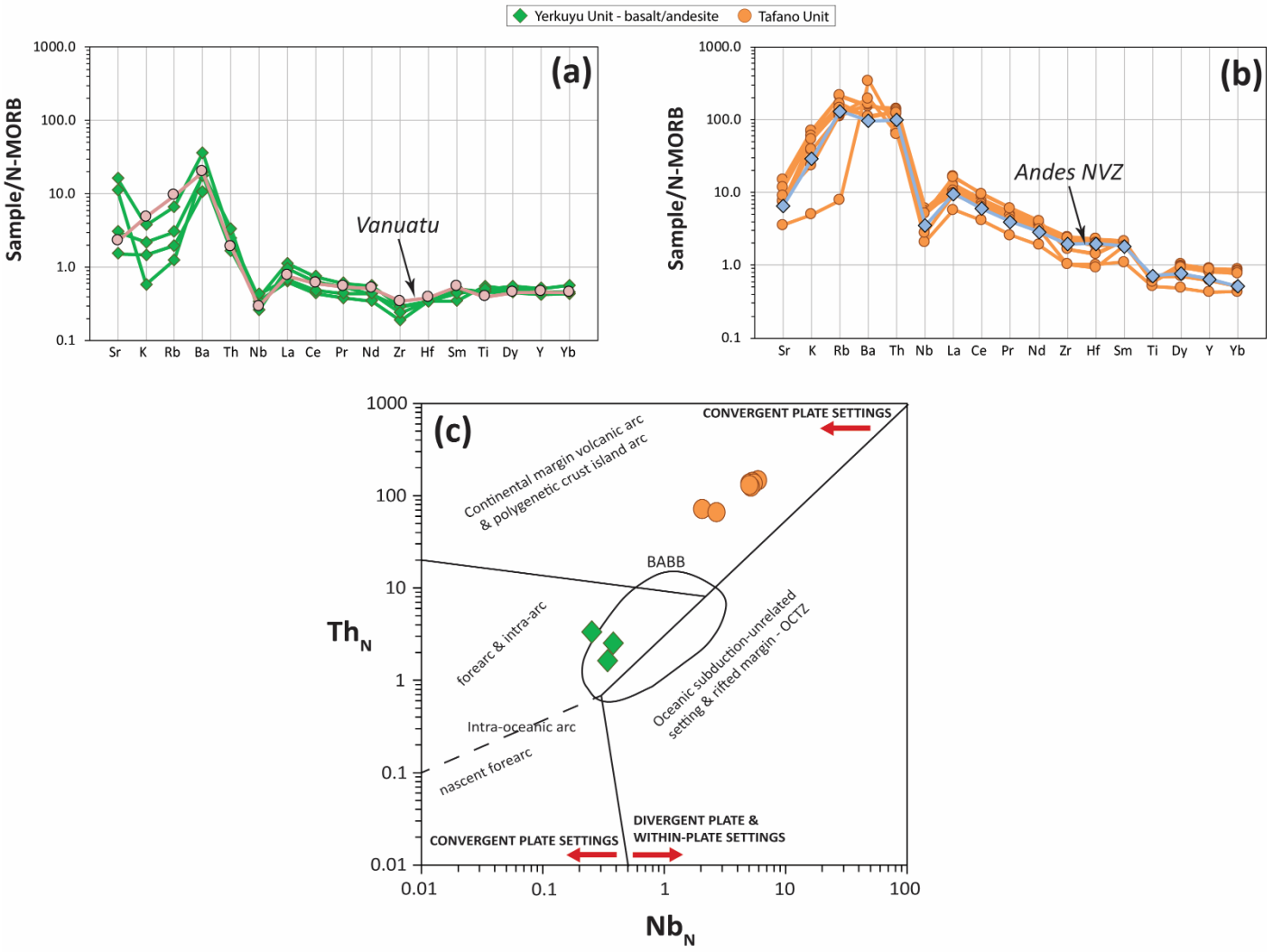
Yerkuyu Unit - basalt/andesite
Tafano Unit
(a)
Sample/N-MORB
1000.0
100.0
10.0
1.0
0.1
Sr K Rb Ba Th Nb La Ce Pr Nd Zr Hf Sm Ti Dy Y Yb
Vanuatu
(b)
Andes NVZ
(c)
Continental margin volcanic arc & polygenetic crust island arc
CONVERGENT PLATE SETTINGS
BABB
forearc & intra-arc
Oceanic subduction-unrelated setting & rifted margin - OCTZ
Intra-oceanic arc
nascent forearc
DIVERGENT PLATE & WITHIN-PLATE SETTINGS
CONVERGENT PLATE SETTINGS
Th_N
Nb_N
1000
100
10
1
0.1
0.01
0.01 0.1 1 10 100

Fig. 10

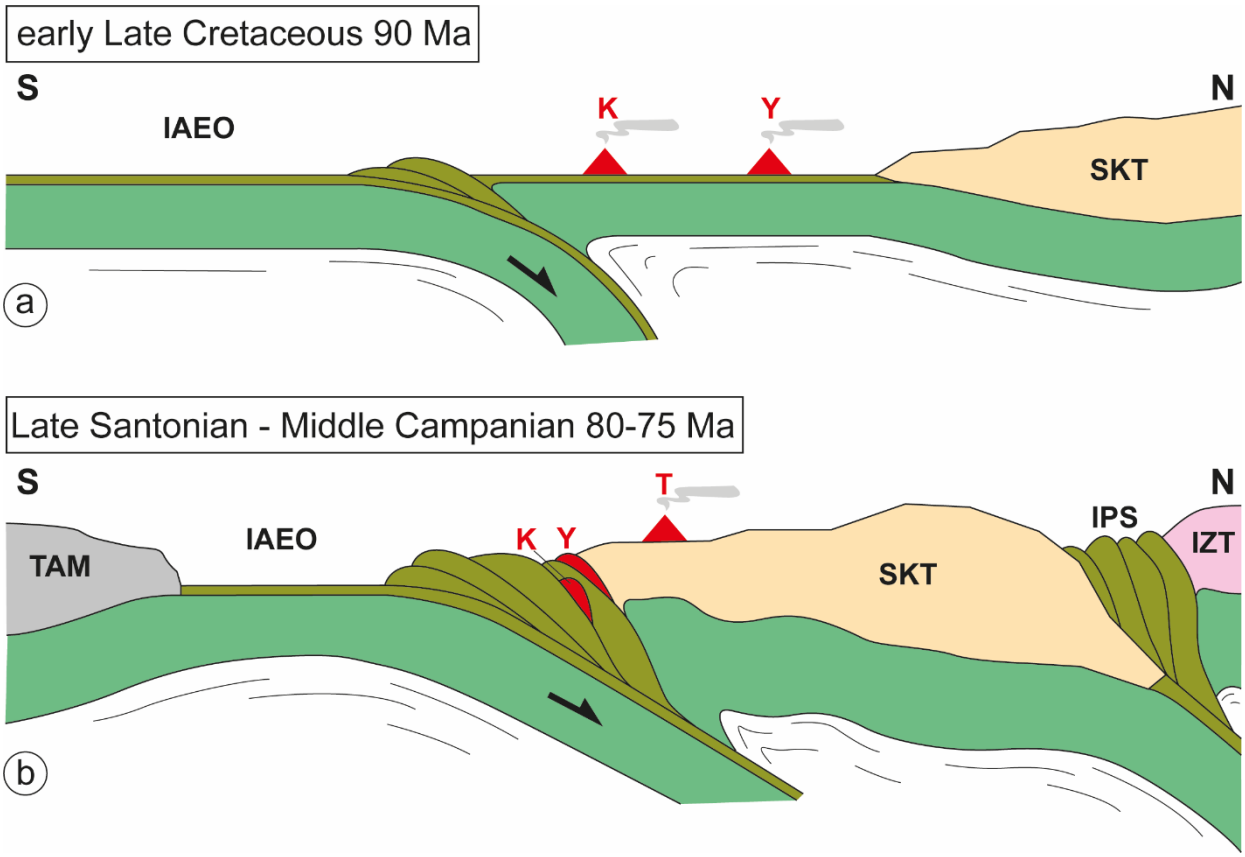
early Late Cretaceous 90 Ma
S
N
IAEO
K
Y
SKT
a
Late Santonian - Middle Campanian 80-75 Ma
S
N
T
IPS
IZT
TAM
IAEO
K
Y
SKT
b

Fig. 11

Table 1. Geochemical data for the studied volcanic rocks from the Tafano and Yerkuyu Units.

Sample	15-TF-12	15-TF-15	15-TF-19B	15-TF-20	15-TF-8	15-TF-11	AET-13	AET-16	IPS-13-59	IPS-13-65	IPS-13-67	IPS-13-79	AET-17	AET-20
Unit	Yerkuyu	Yerkuyu	Yerkuyu	Yerkuyu	Yerkuyu	Yerkuyu	Tafano	Tafano	Tafano	Tafano	Tafano	Tafano	Tafano	Tafano
Lithology	basalt	andesite	andesite	andesite	dacite	dacite	basaltic andesite	basaltic andesite	basaltic andesite	basaltic andesite	basaltic andesite	basaltic andesite	andesite	andesite
Coordinates	40°55'40" N 33°42'38" E	40°56'14" N 33°43'14" E	40°54'30" N 33°46'00" E	40°54'38" N 33°45'27" E	40°54'16" N 33°43'24" E	40°55'30" N 33°42'33" E	40°50' 11" N 33°57'34" E	40°50' 11" N 33°57'34" E	40°50'32'' N 33°57'46'' E	40°49'07'' N. 33°56'33'' E	40°49'07'' N. 33°56'33'' E	40°51'44'' N 34°05'39'' E	40°50' 46" N 33°57'46" E	40°50' 46" N 33°57'46" E
SiO_2	47.05	47.88	53.50	54.73	70.23	69.96	51.18	52.26	56.42	51.90	51.55	44.93	48.86	49.35
Al_2O_3	16.79	18.14	17.10	14.81	13.48	13.56	17.72	17.40	16.53	17.04	18.04	17.79	20.56	20.44
Fe_2O_{3T}	10.60	10.67	9.88	9.94	4.02	3.98	8.80	8.40	8.26	8.63	7.77	10.57	9.43	9.19
MgO	7.37	3.67	4.21	3.68	1.77	1.56	4.27	4.25	4.42	4.25	4.35	5.11	2.56	2.54
CaO	10.20	12.70	6.45	6.36	2.77	3.13	5.74	5.10	3.99	5.48	6.88	6.53	8.73	8.61
Na_2O	2.33	1.49	2.76	3.71	4.23	3.28	3.01	3.16	3.77	3.59	3.54	5.29	3.10	3.14
K_2O	0.26	0.04	0.15	0.10	0.31	1.34	4.80	5.01	0.34	4.19	3.78	1.61	2.71	2.74
TiO_2	0.55	0.56	0.66	0.60	0.36	0.40	0.75	0.74	0.62	0.74	0.80	0.81	0.73	0.73
P_2O_5	0.03	0.02	0.02	0.03	0.07	0.06	0.33	0.31	0.23	0.31	0.34	0.45	0.31	0.32
MnO	0.18	0.13	0.15	0.11	0.05	0.11	0.12	0.11	0.05	0.11	0.12	0.22	0.15	0.17
Cr_2O_3	0.015	0.003	bdl	0.005	bdl	bdl	0.002	0.002	0.012	0.004	0.005	0.007	bdl	bdl
LOI	4.2	4.4	4.9	5.8	2.6	2.5	2.9	2.8	5.0	3.4	2.5	6.3	2.5	2.4
Sum	99.60	99.72	99.79	99.83	99.91	99.89	99.56	99.57	99.61	99.65	99.69	99.60	99.66	99.65
Ni	55.1	26.6	8.9	19.7	4.7	2.6	9.2	9.9	21.1	9.2	11.4	17.2		
Co	45.8	33.8	27.5	26.9	7.8	7.8	22.9	24.4	31.8	27.2	26.3	34.4	24.8	25.7
Sc	38	37	44	46	11	14	23	22	15	22	24	23	13	12
V	280	360	373	363	61	83	217	216	154	208	208	302	167	158
Rb	3.7	0.7	1.7	1.1	5.8	20.7	118.0	120.4	4.4	94.0	80.6	67.8	62.9	64.8
Sr	1444.3	1005.7	271.4	136.6	165.4	131.3	1338.7	1361.1	319.6	1050.7	676.1	820.0	669.6	688.7
Ba	228	122	112	66	140	367	956	978	2180	672	711	1236	1028	1047
Hf	0.7	0.7	0.7	0.7	3.7	2.9	4.7	4.2	2.1	3.8	4.0	1.9	3.0	2.9
Nb	0.9	0.6	0.8	1.0	4.0	3.7	14.1	12.7	4.9	12.0	13.0	6.5	12.3	12.1
Ta	bdl	bdl	bdl	bdl	0.4	0.2	0.8	0.8	0.3	0.7	0.7	0.3	0.7	0.7
Zr	21.9	21.2	13.9	17.7	116.6	96.9	182.2	172.9	76.3	165.7	175.2	76.7	124.0	122.9
Y	12.8	11.8	13.0	14.4	29.2	31.3	25.2	25.3	12.0	23.9	22.8	17.5	23.1	24.8
La	2.8	2.4	1.6	1.7	14.0	10.0	32.4	31.0	14.4	26.7	24.4	23.8	41.6	40.6

Ce	5.6	4.7	3.3	3.6	22.9	19.4	59.4	57.2	31.0	52.6	52.0	47.4	69.8	72.3
Pr	0.80	0.72	0.50	0.58	3.51	2.73	7.05	6.66	3.44	6.04	6.35	5.64	8.03	8.07
Nd	4.2	3.2	2.6	3.3	15.4	11.8	27.5	26.5	14.4	24.1	25.9	23.5	29.0	30.8
Sm	1.36	1.20	0.91	1.15	3.62	3.08	5.66	5.33	2.89	5.10	5.20	4.79	5.69	5.64
Eu	0.52	0.43	0.41	0.45	0.83	0.87	1.37	1.38	0.79	1.25	1.25	1.22	1.49	1.54
Gd	1.82	1.61	1.67	1.89	4.44	4.23	5.58	5.25	2.62	4.79	5.02	4.29	5.15	5.16
Tb	0.34	0.33	0.32	0.37	0.77	0.80	0.80	0.77	0.40	0.71	0.76	0.59	0.75	0.72
Dy	2.18	2.04	2.29	2.50	4.90	4.99	4.69	4.52	2.23	4.24	4.32	3.23	4.30	4.25
Ho	0.46	0.48	0.52	0.52	1.04	1.15	0.87	0.87	0.47	0.88	0.81	0.63	0.84	0.79
Er	1.41	1.34	1.57	1.64	3.07	3.56	2.69	2.54	1.36	2.38	2.45	1.57	2.39	2.44
Tm	0.22	0.21	0.23	0.25	0.44	0.52	0.40	0.38	0.19	0.37	0.36	0.25	0.36	0.34
Yb	1.31	1.32	1.39	1.73	2.37	3.41	2.67	2.58	1.32	2.46	2.38	1.54	2.33	2.37
Lu	0.21	0.21	0.25	0.28	0.39	0.54	0.43	0.41	0.20	0.37	0.40	0.24	0.36	0.35
Th	0.3	0.4	0.2	bdl	3.2	2.6	17.1	16.4	8.3	15.5	15.6	7.7	14.7	14.8
U	0.1	bdl	0.2	0.1	0.3	0.9	6.9	6.6	1.6	4.8	6.2	3.2	3.9	3.5
Pb	0.6	0.8	1.5	0.4	5.5	1.5	13.8	15.8	5.5	13.1	6.8	7.3	7.0	6.6
Zr/Nb	24.3	35.3	17.4	17.7	29.2	26.2	12.9	13.6	15.6	13.8	13.5	11.8	10.1	10.2
Th/Nb	0.33	0.67	0.25	-	0.80	0.70	1.21	1.29	1.69	1.29	1.20	1.18	1.20	1.22
La/Nb	3.11	4.00	2.00	1.70	3.50	2.70	2.30	2.44	2.94	2.23	1.88	3.66	3.38	3.36
Nb/Yb	0.69	1.69	2.69	3.69	4.69	5.69	6.69	7.69	8.69	9.69	10.69	11.69	12.69	13.69
Th/Yb	0.23	0.30	0.14	-	1.35	0.76	6.40	6.36	6.29	6.30	6.55	5.00	6.31	6.24
Dy/Yb	1.66	1.55	1.65	1.45	2.07	1.46	1.76	1.75	1.69	1.72	1.82	2.10	1.85	1.79

$Fe_2O_{3\ tot}$ = total iron; bdl = below detection limit. The Tafano Unit data are from Ellero et al. (2015b).